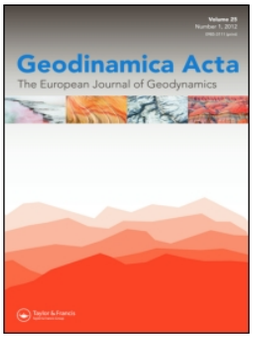

Geodinamica Acta

ISSN: 0985-3111 (Print) 1778-3593 (Online) Journal homepage: https://www.tandfonline.com/loi/tgda20

On the geodynamics of the Alpine collisional granitoids from Central Anatolia: petrology, age and isotopic characteristics of the granitoids of the Ekecikdağ Igneous Association (Aksaray/Turkey)

Fatma Toksoy-Köksal

To cite this article: Fatma Toksoy-Köksal (2019) On the geodynamics of the Alpine collisional granitoids from Central Anatolia: petrology, age and isotopic characteristics of the granitoids of the Ekecikdağ Igneous Association (Aksaray/Turkey), Geodinamica Acta, 31:1, 1-26, DOI: 10.1080/09853111.2019.1597677

To link to this article: https://doi.org/10.1080/09853111.2019.1597677

© 2019 The Author(s). Published by Informa UK Limited, trading as Taylor & Francis Group.

Published online: 25 Apr 2019.

Submit your article to this journal

Article views: 828

View related articles

View Crossmark data

Full Terms & Conditions of access and use can be found at
https://www.tandfonline.com/action/journalInformation?journalCode=tgda20

GEODINAMICA ACTA
2019, VOL. 31, NO. 1, 1–26
https://doi.org/10.1080/09853111.2019.1597677

Taylor & Francis
Taylor & Francis Group

ARTICLE

OPEN ACCESS Check for updates

On the geodynamics of the Alpine collisional granitoids from Central Anatolia: petrology, age and isotopic characteristics of the granitoids of the Ekecikdağ Igneous Association (Aksaray/Turkey)

Fatma Toksoy-Köksal

Dept. of Geological Engineering, Middle East Technical University, Ankara, Turkey

ABSTRACT

Granitoids of the Ekecikdağ Igneous Association (Central Anatolia/Turkey) are products of collisional–post-collisional magmatism in the Ekecikdağ area. These granitoids are granodiorite, microgranite and leucogranite. Field relations of granodiorites with microgranites is obscured, but leucogranites intrude both rock types. Mean zircon laser ablation (LA)-ICP-MS ^{206}Pb-^{238}U ages of granodiorites and microgranites are 84.52 ± 0.93 Ma and 80.7 ± 1.6 Ma, respectively, and age of leucogranites is suggested as 80 Ma, based on field relations combined with $^{206}Pb/^{238}U$ and Rb-Sr ages. Crystallisation temperatures of granodiorites, microgranites and leucogranites are 728°C-848°C, 797°C-880°C, 704°C-809°C, respectively.

Geochemical characteristics including Sr-Nd isotopic evidences infer a non-cogenetic character, as there is a high crustal contribution in I-type granodiorite sources, a crustal source with insignificant and significant mantle inputs in S-type microgranites and leucogranites, respectively. LA-ICP-MS Lu-Hf isotope data from zircons reveal their crustal nature ($\varepsilon Hf_{(t)}$: −1.3 ± 0.5 to −8.8 ± 0.5). Crustal melting linked to the Alpine thickening during the Late Cretaceous led to formation of heterogeneous sourced granitoids with crustal dominated sources in the Ekecikdağ area. Understanding of the nature and evolution of collisional Ekecikdağ granitoids is not only important to put contribution in the geodynamic evolution of Central Anatolia and surrounding Alpine area, but also to better understand systematics of collisional magmatic systems.

ARTICLE HISTORY
Received 31 January 2019
Accepted 18 March 2019

KEYWORDS
Ekecikdağ Igneous Association; Central Anatolia; Sr-Nd isotope; Zircon U-Pb age; Lu-Hf isotope

1. Introduction

Granitoids are significant for the Alpine geological context since their petrology reflects aspects of closure of oceanic branches and evolution of the continental crust. The last stages of the Alpine orogeny in Central Anatolia (Turkey) left traces behind especially in the igneous rocks formed during these periods. Therefore the petrology of these igneous rocks provides noteworthy information about the crustal evolution of Central Anatolia and its surroundings. There are widespread granitoid intrusions in Central Anatolia, and numerous geological, mineralogical, geochemical and geochronological studies of them have been done (Akıman et al., 1993; Boztuğ, 2000, 2007c, 2007b, 2009, 2008; Boztuğ, Tichomirowa, & Bombach, 2007a; Delibaş, Genç, & De Campos, 2011; Deniz & Kadıoğlu, 2016; Düzgören-Aydın, Malpas, Göncüoğlu, & Erler, 2001; Erler et al., 1991; Göncüoğlu, Köksal, & Floyd, 1997a; Görür, Oktay, Seymen, & Şengör, 1984; Güleç & Kadıoğlu, 1998; İlbeyli, 2005; İlbeyli, Pearce, Thirlwall, & Mitchell, 2004; Kadıoğlu, Ateş, & Güleç, 1998; Kadıoğlu, Dilek, & Foland, 2006; Kadıoğlu, Dilek, Güleç, & Foland, 2003; Köksal, Möller, Göncüoğlu, Frei, & Gerdes, 2012; Köksal, Romer, Göncüoğlu, & Toksoy-Köksal, 2004; Köksal et al., 2013; Yalınız, Aydın, Göncüoğlu, & Parlak, 1999). However, there is no consensus on the petrology of the granitoids and their role in the geodynamic evolution of the region. One group of scientists advocates the existence of the Inner Tauride Suture separating the Tauride block from the Anatolide block (Deniz & Kadıoğlu, 2016; Görür et al., 1984; Kadıoğlu et al., 2003; Okay et al., 1996; Şengör & Yılmaz, 1981). These authors linked the generation of the Central Anatolian Crystalline Complex (CACC) granitoids with the Andean type arc formed due to the NE dipping subduction zone beneath the CACC through which the Inner Tauride oceanic lithosphere consumed during the Late Cretaceous (e.g. Deniz & Kadıoğlu, 2016; Kadıoğlu et al., 2006, 2003) or in the Paleocene-Early Eocene (e.g. Görür et al., 1984). Another group of scientists opposing the existence Inner Tauride Suture (e.g. Boztuğ et al., 2009; Göncüoğlu, Kozlu, & Dirik, 1997b; Hinsbergen et al., 2016; Köksal et al., 2012, 2013), on the other hand, argue that granitoids in Central Anatolia developed in a collisional to post-collisonal system of the Pontides with the Tauride-Anatolide platform (e.g. Göncüoğlu et al., 1997a, 1997b; Boztuğ, 1998, 2000; Boztuğ et al., 2008, 2009; Tatar & Boztuğ, 1998; Yılmaz & Boztuğ, 1998; Yalınız et al., 1999; İlbeyli et al., 2004; Köksal et al., 2004, 2012, 2013; Delibaş et al., 2011). The

CONTACT Fatma Toksoy-Köksal ftkoksal@metu.edu.tr Dept. of Geological Engineering, Middle East Technical University, Ankara, Turkey

© 2019 The Author(s). Published by Informa UK Limited, trading as Taylor & Francis Group.
This is an Open Access article distributed under the terms of the Creative Commons Attribution License (http://creativecommons.org/licenses/by/4.0/), which permits unrestricted use, distribution, and reproduction in any medium, provided the original work is properly cited.

Ekecikdağ Igneous Association (EIA) (Aksaray) is one of the largest igneous complexes in the western part of the Central Anatolia with an area of more than 200 km^2 with a NW-SE trend (Figure 1). Detailed petrological investigation of the granitoids in this association would provide a substantial contribution to the present knowledge on the western part of the CACC. Previous studies (Göncüoğlu & Türeli, 1994; Toksoy-Köksal, 2016; Türeli, Göncüoğlu, & Akıman, 1993) made available a background on the geological, mineralogical and geochemical aspects of the EIA granitoids. However, geochronological age of the EIA graniotids should be determined to better understand the geodynamic evolution of the region. Moreover, for accurate assessment of the petrology of the EIA granitoids isotopic data is truly substantial. This study aims to provide new insight on the petrogenesis of the EIA, as an example of the collisional igneous complexes in the Alpine realm, by using geochronological, whole rock Sr-Nd and zircon Lu-Hf isotope data.

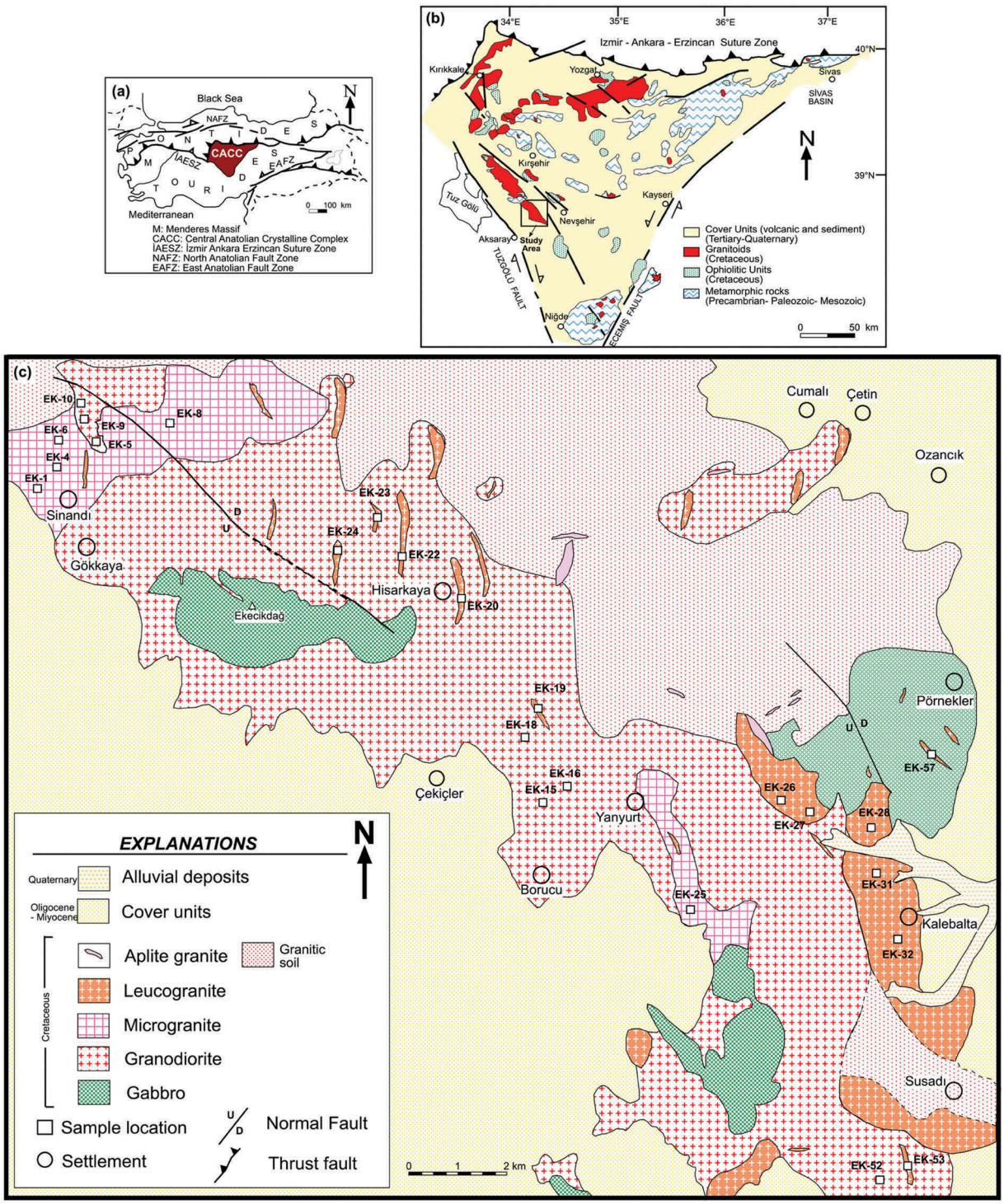

Figure 1. (a) Location of the Central Anatolian Crystalline Complex in the tectonic framework of Anatolia, (b) Location of the Ekecikdağ Igneous Association (EIA) in the Central Anatolian Crystalline Complex (modified from Göncüoğlu et al., 1991), (c) Geological map of the Ekecikdağ area (from Toksoy-Köksal, 2016) and sample locations.

2. Regional geological framework

The metamorphic, granitic and ophiolitic units in Central Anatolia are named as the CACC (Göncüoğlu et al., 1993, 1992, 1997a; Göncüoğlu, Toprak, Kuşçu, Erler, & Olgun, 1991). The basement metamorphic rocks with sedimentary and magmatic protoliths within the CACC are formed from the conjugate rocks of the Precambrian to Upper Mesozoic members of the Tauride stratigraphic successions (Göncüoğlu et al., 1997b; Özgül, 1976). These are paragneisses and orthogneisses and schists with rare carbonate interlayers, which are conjugates of the Precambrian to early Paleozoic Tauride basal succession, and calc-schists to marbles characterising the late Paleozoic and Mesozoic Tauride units at the upper parts. These metamorphic rocks are overthrusted by supra-subduction zone type ophiolitic rocks, and in turn both units are cut by per-aluminous two-mica S-type granitoids (leucogranites) and rare I-type granitoids (granodiorites) (Boztuğ, 2000; Boztuğ et al., 2009, 2008; Göncüoğlu et al., 1993, 1991; İlbeyli, 2005; Köksal & Göncüoğlu, 2008; Yalınız et al., 1999) (Figure 1, for columnar section see Figure 1 in Toksoy-Köksal, Göncüoğlu, & Yalınız, 2001). Subsequent I-type calc-alkaline granitic magmatism (granites and monzonites), on the other hand, form most of the granitic rocks within the CACC (Boztuğ, 1998, 2000; Göncüoğlu et al., 1997a; Köksal et al., 2012, 2013). Relatively rare A-type syenitic rocks (quartz-syenites and foid-syenites) are coeval and/or younger than the I-type granitoids (Boztuğ, 2000; Göncüoğlu et al., 1997a; Köksal, Göncüoğlu, & Floyd, 2001; Köksal et al., 2004; Otlu & Boztuğ, 1998). Moreover, the cover units on the CACC units comprise unmetamorphosed Upper Maastrichtian to Lower Paleocene, Paleocene-Eocene volcanic, volcanoclastic and carbonate rocks, Oligocene-Miocene evaporites and Pliocene to recent sedimentary rocks, volcanoclastic and volcanic rocks (Göncüoğlu et al., 1991; Köksal et al., 2001).

3. Geology

The EIA granitoids are differentiated into four units in previous work (Göncüoğlu & Türeli, 1994; Türeli, 1991; Türeli et al., 1993), namely the Borucu granodiorite-monzogranite, the Hisarkaya porphyry granite, the Sinandı microgranite and the Kalebalta leucogranite. Recent examinations, including field, mineralogical/petrographical characteristics suggest that the Hisarkaya porphyry granite is a subunit of the Borucu granodiorite-monzogranite, therefore they are evaluated together (Toksoy-Köksal, 2016). The intrusive rock units in the study area are simplified as granodiorite, microgranite and leucogranite as described by Toksoy-Köksal (2016) (Figure 1).

Granodiorites are the main magmatic phase in the study area, and form large spheroidal greyish outcrops. It is characterised by phaneritic texture with abundant biotite and amphibole contents and coarse K-feldspar crystals in the field (Figure 2(a)). Sub-angular to rounded mafic microgranular enclaves are also characteristic of the granodiorites (Figure 2(b)). In the study area, especially in the northeastern part, there are no in-situ granitic outcrops. The loose soil in this area, however, is very different from the Oligocene-Miocene cover units, and consists of minerals, especially K-feldspar existing in the granodiorite. Hence these areas are mapped as granitic soil that is formed by decomposition of the granodiorite (Figure 1).

Microgranites are found in the NW of the study area, near Sinandı and Gökkaya villages and in the east near Yanyurt village (Figure 1). They are characteristically dark grey and microgranular with abundant biotite (Figure 2(c)), and are cut by the leucogranites (Figure 2(d)), but their relation with the granodiorites is obscured in the field by the cover units.

Leucogranites, equigranular, pinkish white and with limited mafic mineral content, cut both the microgranites and granodiorites (Figure 2(d,e)).

Gabbroic rocks in the study are intruded by the Ekecikdağ granitoids, and are described as dismembered ophiolitic rocks as in other parts of the CACC (e.g. Koçak, Isık, Arslan, & Zedef, 2005; Köksal, Toksoy-Köksal, & Göncüoğlu, 2017; Toksoy-Köksal et al., 2001; Toksoy-Köksal, Oberhaensli, & Göncüoğlu, 2009; Yalınız et al., 1999). The field relation of the granitoids with the metamorphic basement units is not observed in the study area. However, in nearby regions, intrusive contacts of the granodiorites and the leucogranites with the metamorphic rocks of the CACC can be observed. The cover units are Oligocene-Miocene horizontally layered fine-grained clayey-tuffaceous lacustrine deposits.

4. Petrography

The petrographical characteristics of the granitoids, along with their mineral chemistry data, were presented in detail by Toksoy-Köksal (2016). Here the summary of the petrographical features are given. Amphibole with ferro- and magnesio-hornblende composition is exclusively observed in the granodiorites. In addition, the granodiorites consist of quartz, orthoclase (generally kaolinized subhedral, perthitic crystals with Or_{85-98} composition), plagioclase (rarely serizited, zoned subhedral with An_{15-49} content), biotite (rarely chloritized, subhedral, transitional to Mg-biotite) as main phases with zircon, titanite, allanite (having euhedral crystals up to 1 mm in size), apatite and opaque minerals as

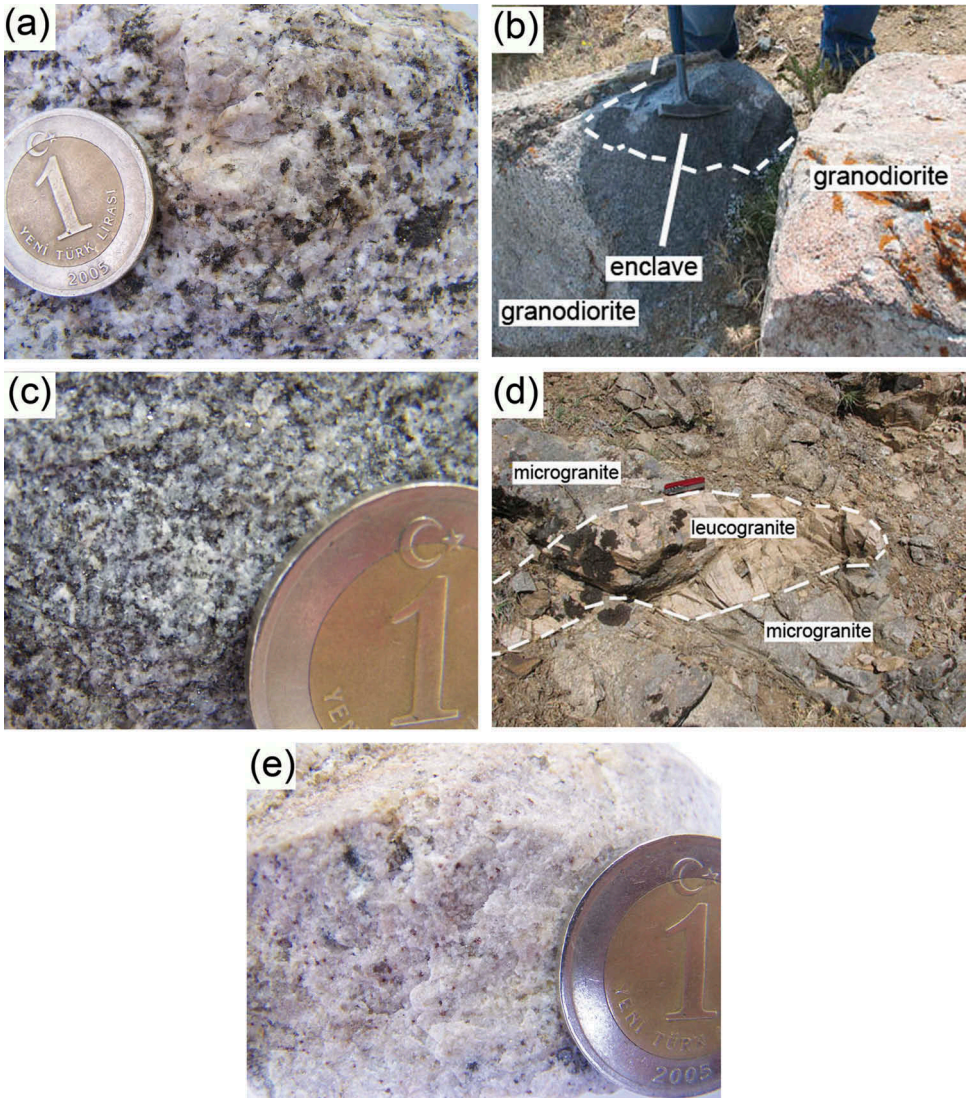

Figure 2. Close up view of (a) the granodiorite with alkali-feldspar phenocrysts including hornblende crystals, (b) mafic microgranular enclave in the granodiorite, (c) the microgranite, (d) the leucogranite intruding the microgranite and (e) the mafic mineral poor leucogranite.

accessory phases (Figure 3(a)). K-feldspar phenocrysts produce a porphyritic texture. Hornblende-dominant microgranular enclaves are frequently observed within the granodiorites.

The microgranite is made up of quartz, orthoclase (kaolinized carlsbad-type twinned subhedral, $Or_{85\text{-}98}$ composition), microcline (generally kaolinized, microcline-type twinned subhedral), plagioclase (generally serizitized albite-type twinned and zoned subhedral crystals with $An_{17\text{-}62}$ composition), biotite (rarely chloritized subhedral, Fe-biotite) and muscovite (petrographically both primary and secondary origin) displaying microphaneritic texture (Figure 3(b)). Micrographic and myrmekitic textures are also developed in these rocks.

The leucogranites are composed of quartz, orthoclase (kaolinized subhedral crystals with $Or_{85\text{-}98}$ content), plagioclase (albitic twinned euhedral/sub-hedral crystals with $An_{1\text{-}17}$ content), biotite (Fe-biotite) as major minerals, and muscovite with apatite, zircon and opaque minerals as accessory minerals displaying granitic and micrographic textures (Figure 3(c)). Zircons are zoned and in contact with biotite, quartz, orthoclase and plagioclase.

5. Analytical methods

In the scope of this study, 5 microgranite, 5 granodiorite, 12 leucogranite and 2 mafic microgranular enclave samples were analysed for whole-rock geochemistry in Acme Analytical Laboratories (Canada) and Central Laboratory of Middle East Technical University (Turkey). A subset of these samples, five from microgranites, five from granodiorites and four from leucogranites were also analysed for their whole-rock Sr and Nd isotope ratios. Moreover, on zircon crystals, LA-SF-ICP-MS U-Pb age measurements were performed at the Geological Survey of Denmark and Greenland (GEUS, Denmark) and Lu-Hf isotope analyses at the Goethe-University Frankfurt (Germany).

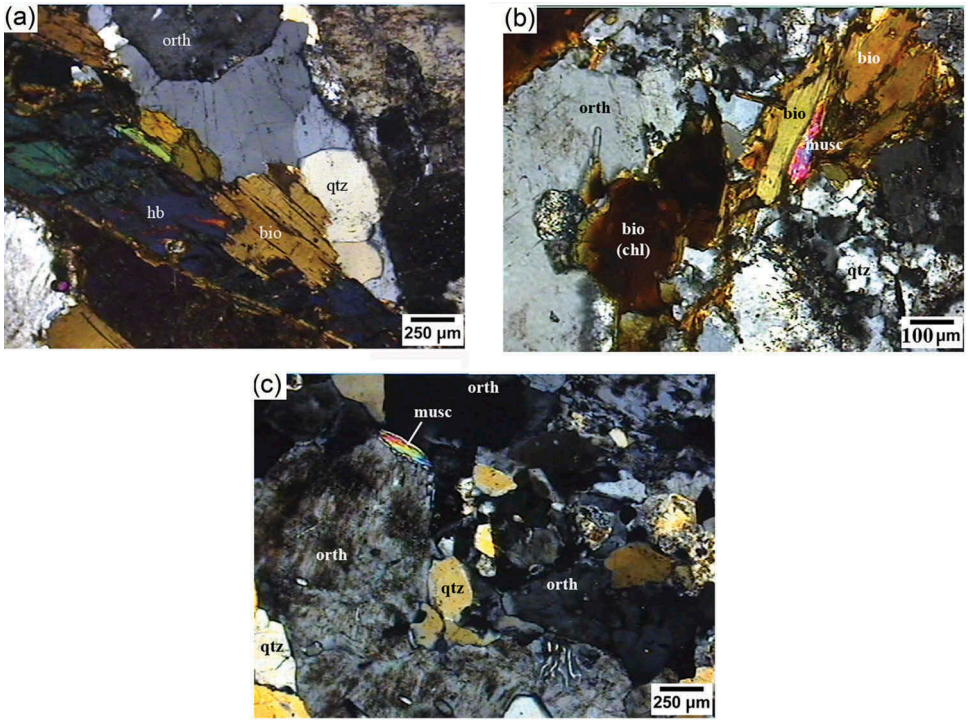

Figure 3. General petrographical view of (a) the granodiorite containing hornblende, plagioclase, quartz, orthoclase, biotite, (b) two mica microgranite with biotite and muscovite, and quartz, orthoclase, microcline, plagioclase and (c) primary muscovite in the leucogranite (hb: hornblende, bio: biotite, musc: muscovite, plag: plagioclase, orth: orthoclase, qtz: quartz).

Major, trace and rare earth elements (REE) are measured after $LiBO_2/Li_2B_4O_7$ fusion with ICP-AES, and after acid digestion (HNO_3 5%) with ICP-MS. Detection limits are 0.01 wt. % for SiO_2, Al_2O_3, MgO, CaO, Na_2O, K_2O, MnO, TiO_2, 0.04 wt. % for Fe_2O_3, 0.001–0.002 wt. % for P_2O_5 and Cr_2O_3 and 0.10 wt. % for LOI. Detection limits for trace and REE are 8 ppm in V, 1 ppm in Ba, 0.5 ppm in Sr, Gd and W, 0.3 ppm in Nd, 0.1 ppm in Cs, Hf, Nb, Rb, Ta, U, Y, Zr, Th, La and Ce, 0.05 ppm in Sm, Dy, Yb, 0.03 ppm in Er, 0.02 ppm in Pr, Eu and Ho, 0.01 ppm in Tb, Tm, Lu. Analytical precision is about 0.05–0.15% for major elements, and 0.5 to 1.5% in trace elements and REE.

Strontium (Sr) and (Neodymium) Nd isotope analyses were performed at the Radiogenic Isotope Laboratory of Central Laboratory/Middle East Technical University (METU), (Ankara) after the methods described by Köksal et al. (2017). Isotopic ratios were measured with a Thermo-Fisher Triton TIMS. Strontium is enriched through 2 ml volume BioRad AG50 W-X8 (100–200 mesh) resin with 2.5 N HCl. REE are collected with 6 N HCl following Sr chromatography. Strontium is loaded on single Re filaments with Ta-activator and dilute H_3PO_4. Neodymium is separated from other REE in 2 ml HDEHP (bis-ethyexyl phosphate) coated biobeads (BioRad) resin with 0.22 N HCl. Neodymium is loaded on double filaments with dilute H_3PO_4. $^{86}Sr/^{88}Sr$ ratios are normalised to $^{86}Sr/^{88}Sr = 0.1194$. NIST SRM 987 standard was measured as $^{87}Sr/^{86}Sr = 0.710249 \pm 12$ ($n = 5$). $^{143}Nd/^{144}Nd$ ratios are normalised with $^{143}Nd/^{144}Nd = 0.7219$ and La Jolla Nd standard was measured as $^{143}Nd/^{144}Nd = 0.511846 \pm 5$ ($n = 3$). No bias correction was applied for Sr and Nd analyses. Quality control of the isotope analyses was checked by applying the same procedures to the USGS rock standards. During the period of analyses, the AGV-1 USGS standard gave $^{87}Sr/^{86}Sr = 0.703993 \pm 12$ ($n = 2$) and $^{143}Nd/^{144}Nd = 0.512784 \pm 3$ ($n = 2$) and the G2 USGS standard gave $^{87}Sr/^{86}Sr = 0.709775 \pm 10$ ($n = 2$) and $^{143}Nd/^{144}Nd = 0.512224 \pm 3$ ($n = 2$), respectively.

Detailes of U-Pb geochronology were given in Köksal et al. (2012), Köksal et al. (2013) and Gürsu et al. (2015). Zircon crystals were obtained through standard concentration methods (i.e. crushing, grinding, sieving, heavy mineral concentration by water table, heavy liquids and electro-magnetic procedures, hand-picking under microscope), mounted in epoxy, polished up to half thicknesses and their back-scattered electron (BSE) images were taken by using a Philips XL 40 SEM at GEUS. In-situ LA-SF-ICP-MS U-Pb zircon measurements were performed on a ThermoFinnigan Element2 high resolution magnetic sector field ICP-MS coupled with a Merchantek New Wave 213 nm UV laser ablation system at the Geological Survey of Denmark and Greenland (GEUS) from pre-evaluated spots on the selected grains regarding their rim/core structures and absence of secondary effects like recrystallisation. Lutetium–Hafnium isotope analyses, on the other hand, were performed at Goethe-University Frankfurt with a Thermo-Finnigan Neptune multi-collector ICP-MS by static multicollection during 60 s of ablation with a

spot size of 40 µm on selected grains after evaluation of U-Pb data. Discordance percentages of the U-Pb analyses were determined from the following formula;

$$\text{Discordance } \% = \left(1 - \left[\left({}^{207}\text{Pb}/{}^{235}\text{Udate}\right)/\left({}^{206}\text{Pb}/{}^{238}\text{Udate}\right)\right]\right) * 100 \text{ for the } {}^{206}\text{Pb}/{}^{238}\text{U ages} < 1.0\,\text{Ga}$$

$$\text{Discordance } \% = \left(1 - \left[\left({}^{207}\text{Pb}/{}^{206}\text{Pbdate}\right)/\left({}^{206}\text{Pb}/{}^{238}\text{Udate}\right)\right]\right) * 100 \text{ for the } {}^{206}\text{Pb}/{}^{238}\text{U ages} > 1.0\,\text{Ga}$$

6. Results

6.1. Geochronology

LA-SF-ICP-MS results and Cathodoluminescence (CL) images of the spots and their $^{206}Pb/^{206}U$ ages are given in Table 1 and Figures 4–9.

Granodiorites: The analysed zircon crystals have generally long prismatic with rare short prismatic forms, and their habits are euhedral to subhedral with oscillatory zoning, which includes inherited cores (Figure 4). Ten spots from nine zircons have high discordia % (> 10 %) and their U and Pb contents are extremely high, with values that range respectively from 267 to 7091 ppm and 3 to 93 ppm (Table 1). In the remaining spots U and Pb values have discordance % lower than 10 %, and vary respectively from 65 to 749 ppm and 2 to 43 ppm (Table 1). Th/U ratios of the analysed spots having low discordia % (< 10) vary from 0.11 to 2.41. The rim and core ages of the analysed spots range between 83.0 ± 2.0 Ma and 762 ± 27 Ma. On the $^{206}Pb/^{238}U$-$^{207}Pb/^{235}U$ concordia diagram, no concordant age has been determined (Figure 5) but the weighted ages of the 12 spots indicate 84.52 ± 0.93 Ma (MSWD = 1.3) (Figure 5), and are evaluated as the crystallisation age of the granodiorites.

Microgranites: 26 spots on 14 zircons are measured during U-Pb dating analyses of the microgranites. Three spots discordia % on three zircons exceed 10 % and cannot be used in the age studies. The analysed zircons are euhedral-subhedral, long to short prismatic, and have well-developed oscillatory zones (Figure 6). Th/U ratios vary from 0.41 to 1.60 indicating a typical magmatic origin. The younger ages from the rims of the selected zircons range from 79.0 ± 2.0 Ma to 86.0 ± 3.0 Ma, whereas the core ages vary from 618 ± 24 to 1008 ± 16 Ma (Table 1). No concordia ages between the younger ages have been determined, but a 80.7 ± 1.6 Ma (MSWD = 2.1 weighted mean age from eight spots is interpreted as reflecting the crystallisation age (Figure 7).

Leucogranites: Fourteen spots on the six long prismatic-euhedral oscillatory zoned zircons were analysed to determine their ages (Figure 8). Only three of the 14 spots have low discordance % (< 10 %) and two of them yield 82.7 ± 1.0 Ma (MSWD = 1.6) concordia ages and the oldest inherited age is determined as 156.0 ± 6.0 Ma in the sample. The condordia age (82.7 ± 1.0 Ma) obtained from two spots is interpreted as their crystallisation age (Figure 9(a)). The determined $^{206}Pb/^{238}U$ age of the leucogranites from two spots are older than the age of the microgranites. The leucogranites, however, cut the microgranites and the granodiorites in the field (Figure 2(d)). Therefore, a further Rb-Sr isochron age was determined as 75.3 ± 4.7 Ma despite having a high MSWD value (Figure 9(b)). The high MSWD value could be due to slight alteration in a sample of the leucogranite. Therefore the oldest crystallisation age for the leucogranites is suggested as 80 Ma and this value is used in the calculation of initial isotopic data.

6.2. Whole-rock geochemistry

Results of whole-rock analyses are presented in Table 2. These data were examined by Toksoy-Köksal (2016) – except enclave samples EK-9 and EK-15 – but in this study the data are re-evaluated with additional interpretations. The mobility of the major elements was checked on basis of the alteration indices proposed by Hughes (1973) and Spitz and Darling (1978). On K_2O+Na_2O versus $(K_2O/(K_2O+Na_2O))*100$ diagram (Hughes, 1973), all granitic samples plotted within the range of the igneous spectrum/weakly altered areas, whereas they are placed within the fresh to weakly altered area on an Al_2O_3/Na_2O versus Na_2O diagram (Spitz & Darling, 1978) (Figure 10). The alteration diagrams indicate that all the samples are free of Na-K metasomatism/alteration that can be used in the further petrogenetic studies.

All the granitoids have high-K calc-alkaline character but their aluminium indexes are different (Toksoy-Köksal, 2016). The granodiorites show metaluminous to peraluminous character, but the microgranites and the leucogranites are peraluminous, with higher ANK/ACNK ratios for the microgranites. On the Zr-TiO_2 diagram (Figure 11(a)), the petrographically described granodiorites and microgranites plot in the granodiorite area, whereas the leucogranites are placed in the granite area (Figure 11(a)). These geochemical based rock types are supported by plots in the granodiorite and granite fields on the R1 versus R2 diagram of the De La Roche, Leterrier, Grandclaude, and Marchal (1980) (Figure 11b). On the SiO_2 versus major element variation diagrams, the leucogranite samples have higher SiO_2, Na_2O, K_2O but lower Al_2O_3, $Fe_2O_3^{(T)}$, MgO, CaO, TiO_2, P_2O_5 contents than the granodiorites

Table 1. LA-ICP-MS U-Pb age data of zircons from the EIA granitoids.

					Atomic Ratios							Ages						
Analyse Nr.	^{207}Pb (cps)	U (ppm)	Pb (ppm)	Th U	$^{207}Pb/^{235}U$	1 σ %	$^{206}Pb/^{238}U$	1 σ %	rho	$^{207}Pb/^{206}Pb$	1 σ %	$^{207}Pb/^{235}U$	2 σ (Ma)	$^{206}Pb/^{238}U$	2 σ (Ma)	$^{207}Pb/^{206}Pb$	2 σ (Ma)	Discordia (%)
Leucogranite																		
EK31.1-1r	4561	234	4	0.87	0.086	2.1	0.0130	1.8	0.84	0.0477	1.2	84	4	84**	3	86	27	-0.09
EK31.1-2c	4561	234	6	1.17	0.161	2.1	0.0245	1.8	0.84	0.0477	1.2	152	6	156	6	85	27	2.74
EK31.2-1r	12800	680	11	0.79	0.088	4.6	0.0121	1.4	0.31	0.0532	4.4	86	8	77***	2	337	100	-11.34
EK31.3-1c	107584	8765	119	0.04	0.164	3.9	0.0125	2.3	0.58	0.0951	3.2	154	12	80***	4	1531	60	-92.48
EK31.4-2r	28653	1269	22	0.21	0.273	5.7	0.0125	2.0	0.35	0.1590	5.3	245	28	80***	3	2445	90	-207.20
EK31.4-1c	31592	3438	61	0.09	0.107	2.4	0.0133	1.5	0.63	0.0584	1.9	103	5	85***	3	546	40	-21.36
EK31.5-1r	10127	661	9	0.38	0.140	2.4	0.0121	1.6	0.68	0.0844	1.8	133	6	77***	3	1302	34	-72.52
EK31.5-2r	9293	904	12	0.48	0.086	2.0	0.0128	1.7	0.84	0.0487	1.1	84	3	82**	3	135	26	-2.20
EK31.5-3c	32784	630	18	0.57	0.663	1.8	0.0153	1.4	0.78	0.3150	1.2	517	19	98***	3	3545	18	-428.72
EK31.6-1r	71648	1934	40	0.17	0.139	2.6	0.0130	1.7	0.65	0.0775	1.9	133	7	84***	3	1134	39	-58.80
EK31.6-2r	27738	1947	28	0.05	0.097	2.7	0.0120	1.5	0.55	0.0588	2.2	94	5	77***	2	560	49	-22.60
Microgranite																		
EK4.1-1r	15005	110	13	1,28	0,832	2,2	0,1007	2,0	0,90	0,0599	0,9	615	27	618	24	601	20	0.59
EK4.2-1r	17733	87	12	0,84	1,033	1,9	0,1136	1,7	0,91	0,0660	0,8	721	27	694	24	806	16	-3.91
EK4.2-2c	13921	82	9	0.75	0.793	2.1	0.0850	1.8	0.89	0.0677	0.9	593	24	526***	19	858	19	-11.30
EK4-3-1c	12513	588	9	0,66	0,089	1,8	0,0134	1,6	0,88	0,0482	0,9	86	3	86*	3	110	20	-0.98
EK4.4-1r	11614	523	7	0,54	0,085	1,8	0,0127	1,6	0,90	0,0488	0,8	83	3	81*	3	137	18	-2.29
EK4.4-2c	9894	492	7	0,72	0,104	2,8	0,0133	1,7	0,60	0,0571	2,2	101	6	85***	3	495	48	-18.70
EK4.5-1r	23028	165	29	0,41	1,774	1,8	0,1768	1,6	0,90	0,0728	0,8	1036	37	1049	34	1008	16	3.97
EK4.5-2r	41452	243	37	1,60	1,223	2,3	0,1224	2,2	0,94	0,0724	0,8	811	38	745	33	998	16	-8.93
EK4.6-1r	10459	556	8	0,74	0,082	2,0	0,0123	1,8	0,89	0,0486	0,9	80	3	79*	3	127	21	-1.97
EK4.6-2c	11942	611	9	0,58	0,086	1,8	0,0130	1,6	0,89	0,0480	0,8	84	3	83*	3	97	19	-0.58
EK4.7-1c	14937	698	10	0,54	0,087	2,0	0,0128	1,7	0,85	0,0495	1,1	85	3	82*	3	170	25	-3.65
EK4.8-1c	10084	395	6	0,54	0,093	2,2	0,0130	1,7	0,76	0,0516	1,5	90	4	83*	3	268	33	-7.88
EK4.9-1c	106226	152	48	0,55	5,053	1,6	0,2750	1,5	0,97	0,1333	0,4	1828	58	1566	48	2141**	7	-36.74
EK4.10-1r	20041	84	16	0,93	1,606	1,8	0,1621	1,7	0,93	0,0719	0,6	973	35	968	33	982	13	-0.43
EK4.11-1r	13347	638	9	0,59	0,083	1,7	0,0125	1,4	0,86	0,0483	0,8	81	3	80*	2	113	20	-1.33
EK4.12-1r	11838	481	7	0,68	0,083	1,8	0,0123	1,6	0,87	0,0492	0,9	81	3	79*	2	156	21	-3.20
EK4.13-1r	12436	626	8	0,57	0,082	1,9	0,0123	1,6	0,88	0,0482	0,9	80	3	79*	3	110	21	-1.26
Granodiorite																		
EK18.1-1c	10648	310	5	0.79	0.096	2.1	0.0133	1.7	0.78	0.0523	1.3	93	4	85*	3	298	30	-9.18
EK18.3-1r	7960	191	3	1.12	0.091	2.0	0.0130	1.5	0.76	0.0506	1.3	88	4	83*	3	221	30	-5.81
EK18.3-2r	7013	105	2	1.69	0.092	2.3	0.0134	1.5	0.67	0.0500	1.7	90	4	86*	3	196	39	-4.61
EK18-4-1r	12387	622	9	0.60	0.086	1.9	0.0128	1.6	0.87	0.0489	0.9	84	3	82*	3	142	22	-2.46
EK18.4-2c	7621	149	3	2.41	0.103	3.0	0.0130	1.4	0.47	0.0575	2.6	99	6	83***	2	509	58	-48.54
EK18.5-1r	45709	1501	27	0.12	0.141	2.2	0.0134	1.4	0.64	0.0765	1.7	134	6	86***	2	1107*	33	-56.39
EK18.6-1r	10763	492	7	0.54	0.089	1.8	0.0131	1.4	0.83	0.0490	1.0	86	3	84*	2	146	23	-2.56
EK18.6-2c	13490	732	10	0.48	0.089	1.7	0.0132	1.4	0.82	0.0488	1.0	87	3	85*	2	137	23	-2.13
EK18.7-1c	49429	296	43	0.65	1.235	1.9	0.1254	1.8	0.96	0.0714	0.5	817	30	762	27	970	10	-7.23
EK18.7-2r	16368	65	10	0.75	1.230	2.4	0.1243	1.6	0.67	0.0718	1.8	815	40	755	25	979	37	-7.82
EK18.9-1r	15417	129	14	0.66	0.839	1.6	0.0966	1.5	0.93	0.0630	0.6	618	20	595	18	707	13	-4.01
EK18.9-2c	12654	60	8	0.72	0.943	1.8	0.1083	1.6	0.85	0.0632	0.9	674	25	663	21	714	20	-1.78
EK18.11-1r-	15173	785	11	0.21	0.092	2.2	0.0124	1.6	0.76	0.0540	1.4	90	4	80***	3	369	32	-12.78
EK18.11-2c	22117	314	16	0.31	0.407	3.1	0.0468	3.0	0.96	0.0630	0.8	347	22	295***	18	709	18	-17.49

(*Continued*)

Table 1. (Continued).

Analyse Nr.	^{207}Pb (cps)	U (ppm)	Pb (ppm)	Th/U	Atomic Ratios $^{207}Pb/^{235}U$	1 σ %	$^{206}Pb/^{238}U$	1 σ %	rho	$^{207}Pb/^{206}Pb$	1 σ %	Ages $^{207}Pb/^{235}U$	2 σ (Ma)	$^{206}Pb/^{238}U$	2 σ (Ma)	$^{207}Pb/^{206}Pb$	2 σ (Ma)	Discordia (%)
EK18.13-1r	14544	724	10	0.43	0.091	1.9	0.0133	1.6	0.84	0.0496	1.0	89	3	85*	3	176	24	-3.77
EK18.13-2c	10499	417	6	0.59	0.091	2.0	0.0134	1.8	0.87	0.0492	1.0	88	4	86*	3	158	24	-2.98
EK18.13-3c	14765	703	10	0.49	0.092	1.8	0.0136	1.5	0.80	0.0494	1.1	90	3	87*	3	169	25	-3.41
EK18.16-1c	63361	169	31	0.18	2.891	1.4	0.1778	1.4	0.97	0.1179	0.3	1380	39	1055	29	1925***	26	-23.52
EK18.16-2r	9996	350	5	0.63	0.095	1.8	0.0134	1.4	0.76	0.0518	1.2	93	3	86*	2	276	27	-8.15
EK18.17-1c	110394	7091	93	0.03	0.096	4.2	0.0123	1.7	0.41	0.0566	3.8	93	8	79***	3	476	85	-18.10
EK18.18-1c	11927	450	7	0.65	0.106	5.1	0.0122	1.9	0.37	0.0631	4.7	103	10	78***	3	712	100	-31.04
EK18.19-1r	12639	518	8	0.72	0.088	2.1	0.0129	1.8	0.86	0.0493	1.1	85	4	83*	3	162	25	-3.29
EK18-19-2c	9050	267	4	0.93	0.102	6.4	0.0117	1.5	0.24	0.0634	6.3	99	13	75***	2	722	133	-31.89
EK18-20-1r	40721	3104	54	0.07	0.098	2.3	0.0133	1.4	0.62	0.0534	1.8	95	4	85***	2	346	41	-11.37
EK18.21-1c	32344	1207	20	0.12	0.099	2.3	0.0117	1.6	0.70	0.0609	1.7	96	4	75***	2	637	36	-22.95
EK18.22-1c	13474	749	11	0.11	0.089	1.7	0.0130	1.4	0.84	0.0499	0.9	87	3	83*	2	189	22	-4.43

* Weighted mean aged used, ** Concordia ages used, *** Discordia % > 10 not used in the interpretations

and the microgranites (Figure 12). The granodiorites and the microgranites have similar SiO_2 contents and nearly overlap also in Al_2O_3, $Fe_2O_3^{(T)}$, MgO, CaO, Na_2O, K_2O contents and $Al_2O_3/Fe_2O_3^{(T)}$. The microgranites, however, have higher TiO_2, P_2O_5 values than the granodiorites (Figure 12). On the diagrams of TiO_2 against $Fe_2O_3^{(T)}/Al_2O_3$, $Fe_2O_3^{(T)}$, MgO and P_2O_5, there are no steady continuous trends observed among the granitoid rocks (Figure 13). The plots against TiO_2 except for P_2O_5 (Figure 13) for the granodiorite and the microgranite give almost parallel trends. As in the Harker diagrams, no well-defined trends are observed from the granodiorites and the microgranites to the leucogranites on the SiO_2 against Rb, Sr, Nb, Th, Zr and La diagrams. In all the variation plots, the leucogranites separate clearly from the others, while no clear relation between the granodiorites and the microgranites is evident. The granitoids other than the leucogranites have roughly similar Rb, La but clear differences in Sr, Nb, Th, Zr (Figure 12). The granodiorites are lower in Sr, Nb, Zr but higher in Th than the microgranites.

The mafic microgranular enclaves within the granodiorites have significantly higher Al_2O_3, $Fe_2O_3^{(T)}$, MgO, CaO, TiO_2 but lower SiO_2, K_2O contents compared to the granodiorites. Na_2O and P_2O_5 contents of the enclaves overlap with those of the host granodiorites. The enclaves are dictinctly separate from the host rocks for Th, La, Zr while they are similar for Rb, Sr, Nb. SiO_2 values of the enclaves are not typical of mafic rocks while lower Th, La, Zr values and Zr/TiO_2 ratios of the enclaves clearly show that they were mafic. SiO_2 contents with not typical mafic composition and similarities of Rb, Sr, Nb to granodiorites clearly infer that the enclaves have been chemically modified by composion of the host granodiorites.

On the Zr/Ti versus Th, Nb, Nb/Th, Nb/Y, Zr/Y, La/Yb diagrams, the granodiorites and the microgranites markedly display different patterns to the leucogranites. The granodiorites and the microgranites, which have similar Zr/Ti values, overlap in ratios of Nb/Y, Zr/Y, La/Yb (Figure 14). However, the granodiorites with lower Nb and higher Th contents have a lower Nb/Th ratio that separates them from the microgranites.

The granitoids commonly exhibit enrichment in Th, U, K, Pb, LREE and depletion in Ba, Nb, Sr, P, Eu, Ti elements with flat middle rare earth element (MREE) and heavy rare earth element (HREE) patterns on the chondrite and primitive mantle normalised spider diagrams (after Sun & Mcdonough, 1989). However, positive and negative element patterns of the leucogranites are pronouncedly different from the microgranites and the granodiorites (Figure 15). The leucogranites have higher Th, U contents, lower LREE and more pronounced negative anomalies in Eu, Ti than the granodiorites and the microgranites (Figure 15). On the chondrite normalised REE diagram, all studied samples show LREE enrichment compared to

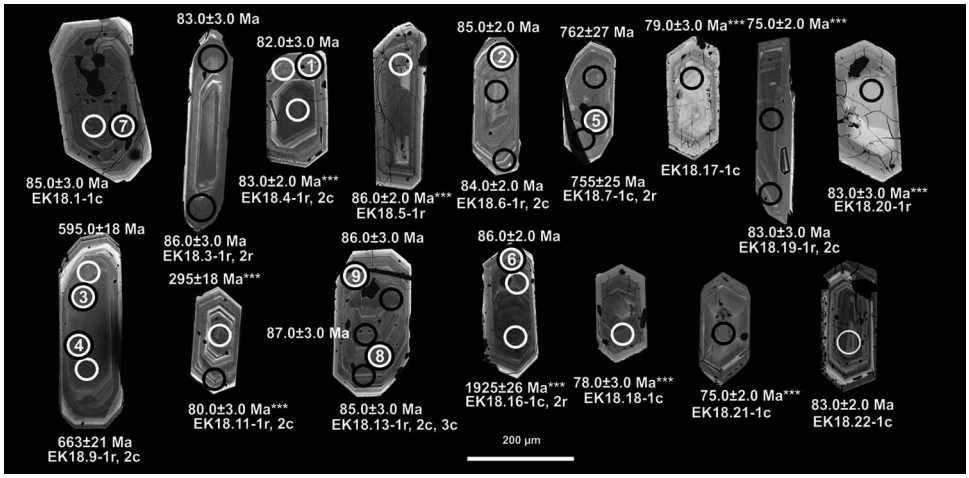

Figure 4. Cathodoluminescence images of zircon crystals from the granodiorites with locations of U-Pb and Lu-Hf analyses. The numbered spots are locations of the Lu-Hf analyses.

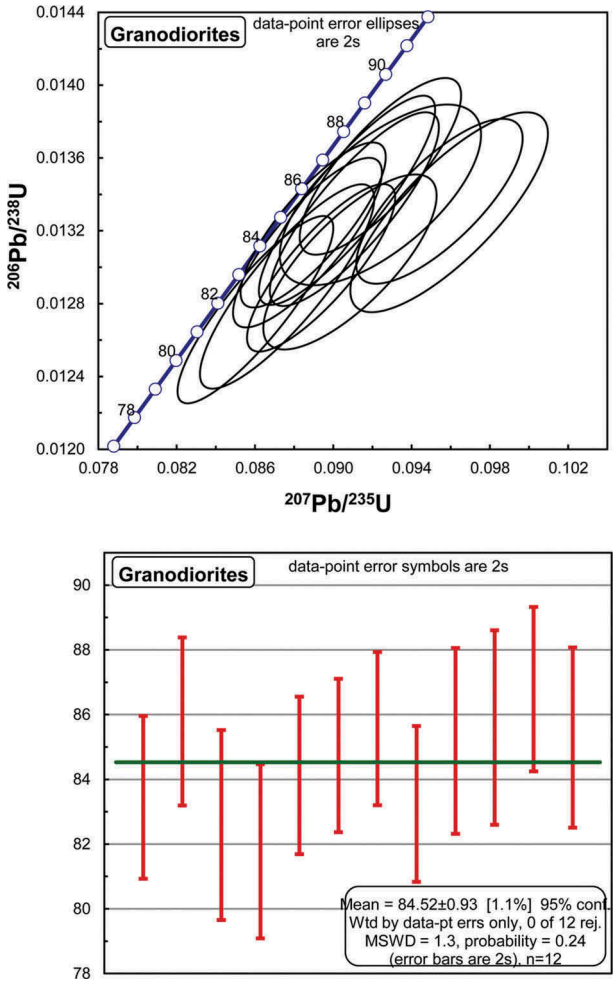

Figure 5. (a) Zircon U-Pb concordia and (b) Mean $^{206}Pb/^{238}U$ age diagrams of the granodiorites.

MREE and HREE. However, the granodiorites and the microgranites have higher enrichment in LREE levels with minor depletion of Eu on a chondrite normalised diagram, whereas the leucogranites with a similar pattern in LREE display lower values with distinctive depletion of Eu. The leucogranites are relatively enriched in HREE (Figure 15). Even though similar enrichment and depletion patterns for both of the microgranites and the granodiorites are present, the microgranites are more enriched in Ba, Sr, P but has lower Th, U, Pb values than the granodiorites. Moreover, the MREE of the microgranites are higher than the granodiorites.

Geochemical plots on tectonic discrimination diagrams by Pearce, Harris, and Tindle (1984), Batchelor and Bowden (1985), Maniar and Piccoli (1989) and Thiéblemont and Cabanis (1990) are used to better understand environments of formation for the granitoids. All of the granitoids plot at the junction point of Volcanic Arc Granites (VAG), Syn-collisional granites (Syn-Colg) and Within Plate Granites (WPG) on the Rb-Nb+Y diagram, that infers a post-collisional system (Figure 16(a)). On the R1-R2 diagram, they are close to syn-collision and post-orogenic areas, whereas they plot within the area of the post-collisional granite area on the Al_2O_3-SiO_2 diagram (Figure 16(b,c)). The granitoids concentrate in the post-collisional/syn-subduction area on the Y-Rb-Nb diagram (Figure 16(d)). To sum up, all of the Ekecikdağ granitoids might have been generated in a collisional to post-collisional system, but they still display differences in geochemical features.

6.3. Whole-rock Sr and Nd isotopes

Strontium-Nd isotopic study was conducted to shed light on the source characteristics (Table 3; Figure 17). The initial $^{87}Sr/^{86}Sr$ and $^{143}Nd/^{144}Nd$ values of the samples are 0.709538–0.712353 and 0.512114–0.512183 for the granodiorites, 0.713279–0.713744 and 0.512086–0.512097 for the microgranites, and 0.707138–0.709765 and 0.512143–0.512230 for the leucogranites, respectively (Table 3). $\varepsilon Nd_{(T)}$ values of the samples range from −6.76 to −8.11 in the granodiorites, −8.62 to −8.75 in the microgranites, and −5.95 to −7.67 in the leucogranites (Table 3). Whole-rock Sr and Nd isotope data from the granitoids display high initial $^{87}Sr/^{86}Sr$ (higher than 0.707) and low εNd values (lower than −5.95) and plot in the

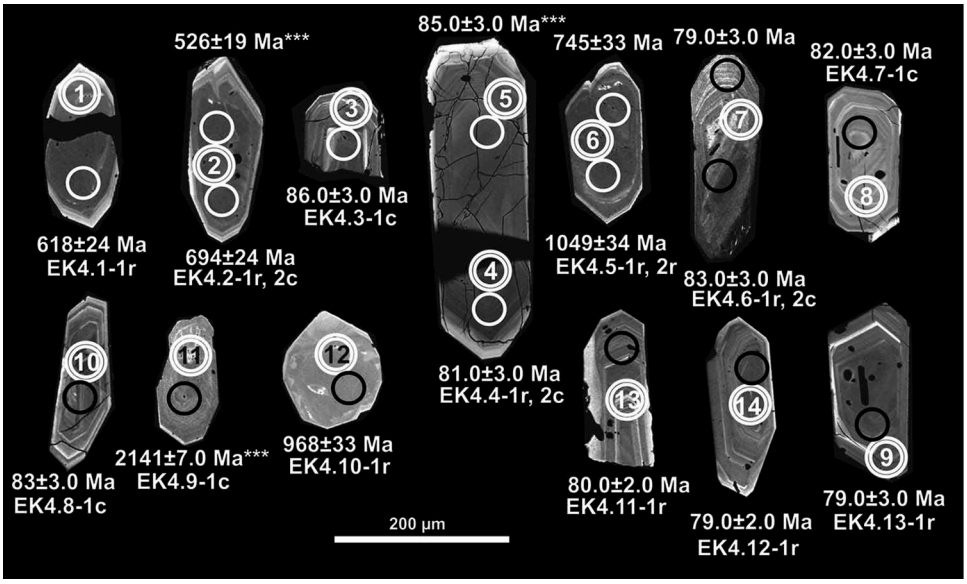

Figure 6. Cathodoluminescence images of zircon crystals from the microgranites with locations of U-Pb and Lu-Hf analyses. The numbered spots are locations of the Lu-Hf analyses.

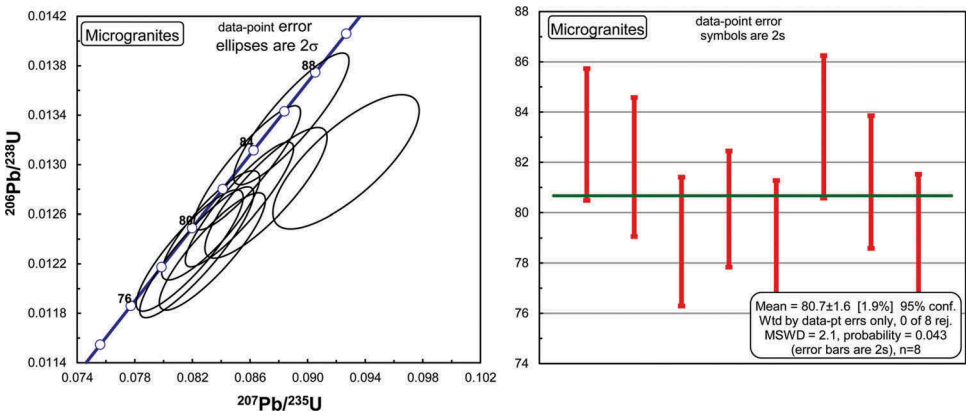

Figure 7. (a) Zircon U-Pb concordia and (b) Mean $^{206}Pb/^{238}U$ age diagrams of the microgranites.

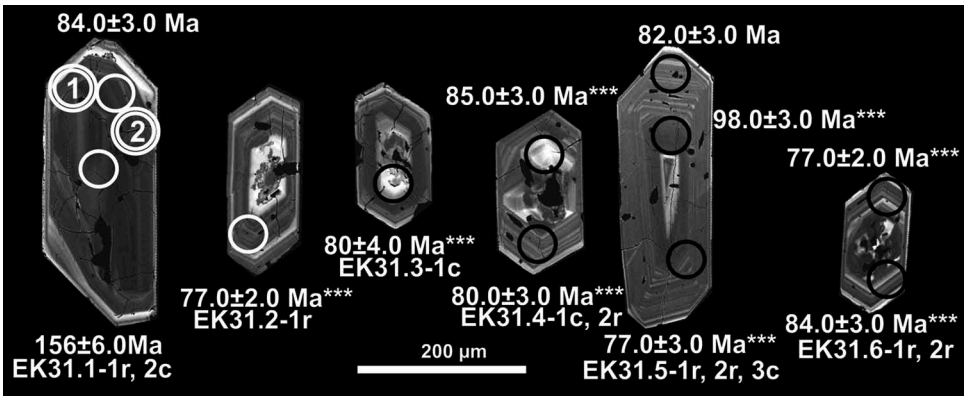

Figure 8. Cathodoluminescence images of zircon crystals from the leucogranites with locations of U-Pb and Lu-Hf analyses. The numbered spots are locations of the Lu-Hf analyses.

area between EMI, EMII and crustal sources (Figure 17). Among the Ekecikdağ granitoids, the microgranites have the most enriched source component, while the leucogranites have the least. Collectively Sr-Nd isotopic data point to enriched sources (Figure 17).

6.4. Zircon Lu-Hf isotope systematics

In-situ LA-MC-ICP-MS Lu-Hf isotope analyses were performed on the selected zircon crystals (Figures 4, 6, 8) from the EIA granitoids. The initial $^{176}Hf/^{177}Hf$ ratios were calculated based on the U-Pb ages of the given

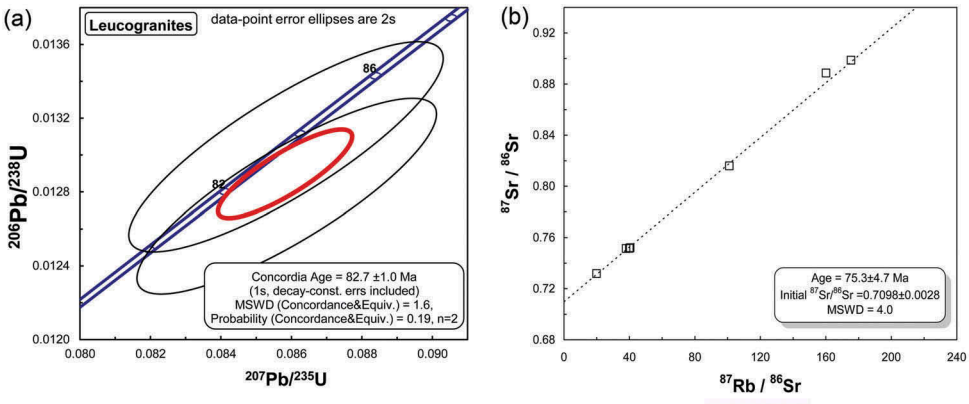

Figure 9. (a) Zircon U-Pb concordia and (b) Rb-Sr isochron of the leucogranites.

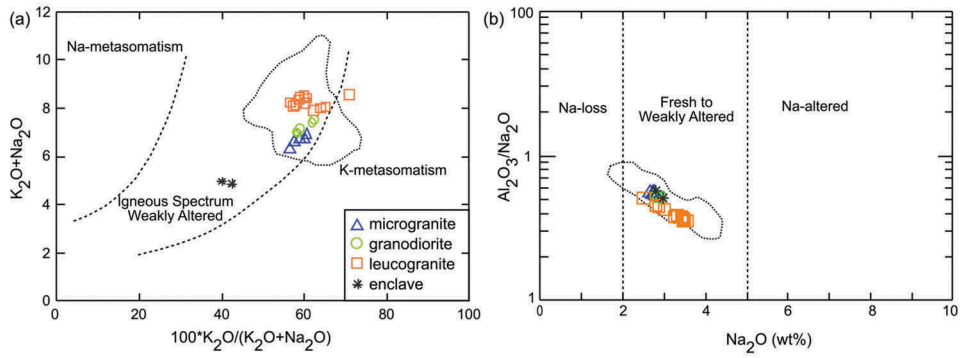

Figure 10. Alteration in the granitoids marked by Na_2O and K_2O loss: (a) K_2O+Na_2O against $(K_2O/(K_2O+Na_2O))*100$ diagram (Hughes, 1973) and (b) Al_2O_3/Na_2O against Na_2O diagram (Spitz & Darling, 1978). The area defined by dashed line represent the data compiled from the Ağaçören Intrusive Suite granitoids (9 samples from Kadıoğlu et al., 2003; 18 samples from Kadıoğlu et al., 2006; 6 samples from Köksal et al., 2012).

points, and results are presented in Table 4. The low initial $^{176}Hf/^{177}Hf$ ratios along with low $\varepsilon Hf_{(t)}$ values (i.e. <0.28268; <-1.3) infer crustal derived sources (Figure 18). Furthermore, $T_{DM}Hf$ ages corresponding to the Late Cretaceous LA-ICP-MS analyses provide a minimum age for the source material of about 1.08–1.43 Ga, that almost coincides with the $T_{DM}Nd$ ages range of the EIA granitoids (i.e. 1.37–1.60 Ga, Table 3). $T_{DM}Hf$ ages from the inherited zircon analyses, on the other hand, are older, ranging from 1.51 to 2.59 Ga.

6.5. Zircon and apatite saturation temperatures

Determination of crystallisation temperature and pressure of the Ekecikdağ granitoid is difficult due to limited mineral assemblages suitable for geothermobarometric calculations. Despite the limitations, geothermometric calculations were conducted by Toksoy-Köksal (2016) that resulted in magmatic to sub-solidus temperatures (granodiorite: 615–783°C, microgranite: 464–565°C, leucogranite: 456–482°C). In this study, therefore, zircon and apatite saturation temperatures from the whole rock element geochemical data were used to determine the magma tempratures of the studied samples using the formulae of Watson and Harrison (1983) and Harrison and Watson (1984). The zircon saturation temperatures used in this study are assumed to be free of the inheritance in the cores. The zircon saturation tempratures are calculated from the following formula;

$$M = (Na + K + 2Ca)/(Al * Si)$$

$$D_{zr} = 497644/Zr$$

$$T_{zircon\,sat.}(^{\circ}C) = (12900/(\ln(D_{Zr}) + 3.8 + 0.85(M - 1)) - 273.15$$

(Watson & Harrison, 1983)

The apatite temperatures are calculated from the whole rock geochemical data by the following the formula:

$$T_{apatite\,sat.}(^{\circ}C) = ((8400 + 26,400(SiO_2 - 0.5))/\ln(42/P_2O_5) + 3.1 + 12.4(SiO_2 - 0.5)) - 273.15$$

(Harrison & Watson, 1984)

Temperatures from zircon saturation calculations are 750°C–770°C (average 758°C) for the granodiorites, 786°C–808°C (average 797°C) for the microgranites,

Table 2. Whole-rock geochemical data from the Ekecikdag Granitoids (Granitoid types: M-microgranite; G: granodiorite; L: leucogranite; E: enclave).

	EK-1	EK-4	EK-6	EK-8	EK-25		EK-5	EK-10	EK-16	EK-18	EK-52	
Granitoid	M	M	M	M	M	Mean	G	G	G	G	G	Mean
SiO_2 (wt%)	70.6	69.9	71.4	71.0	70.0	70.58	69.2	68.8	69.0	69.0	72.1	69.62
TiO_2	0.36	0.40	0.34	0.37	0.42	0.38	0.27	0.29	0.31	0.32	0.22	0.28
Al_2O_3	14.8	15.1	14.8	15.1	14.9	14.94	15.0	15.1	14.9	14.8	14.2	14.80
Fe_2O_3	2.68	3.14	2.83	3.05	3.33	3.00	3.41	3.64	3.32	3.64	2.53	3.31
MnO	0.06	0.06	0.06	0.06	0.07	0.06	0.06	0.07	0.06	0.06	0.06	0.06
MgO	0.71	0.88	0.65	0.76	0.80	0.76	1.00	1.10	0.98	1.06	0.69	0.97
CaO	2.58	2.62	2.13	2.51	2.81	2.53	2.93	2.94	2.95	3.03	2.15	2.80
Na2O	2.66	2.76	2.72	2.74	2.80	2.74	2.92	2.92	2.81	2.87	2.80	2.86
K2O	4.01	3.95	4.17	3.56	3.78	3.89	4.20	4.06	4.67	4.06	4.58	4.31
P_2O_5	0.12	0.15	0.11	0.12	0.15	0.13	0.06	0.07	0.08	0.09	0.06	0.07
Cr_2O_3	0.02	0.02	0.02	0.03	0.02	0.02	0.03	0.02	0.03	0.05	0.02	0.03
LOI	1.20	0.90	0.60	0.50	0.80	0.8	0.80	0.80	0.80	0.90	0.40	0.74
Sum	99.85	99.81	99.84	99.82	99.83	99.83	99.88	99.87	99.85	99.89	99.85	99.87
Rb (ppm)	126	148	152	133	127	137.2	164	152	163	163	227	174
Sr	217	237	191	226	219	218	143	142	145	142	122	139
Nb	12	13	12	13	15	13	7	7	9	10	10	8.60
Y	20	20	18	21	32	22.2	15	16	15	17	21	16.8
Cs	4.6	38.2	8.1	5.5	9.2	13.12	6.6	5.0	6.1	7.3	11.0	7.20
Ta	0.9	0.9	1.0	1.1	1.1	1.02	0.9	0.7	0.8	0.9	1.2	0.90
Sc	7.0	7.0	7.0	7.0	9.0	7.4	6.0	8.0	6.0	7.0	4.0	6.20
Pb	1.6	6.3	3.8	2.6	3.0	3.50	3.4	3.7	5.1	8.2	9.8	6.04
U	2.2	2.7	2.6	2.8	2.3	2.52	5.0	4.3	6.3	4.8	8.3	5.74
Th	10.9	13.5	12.5	13.8	10.4	12.22	13.4	21.0	27.8	21.2	20.8	20.84
Ni	8.6	5.8	5.7	8.8	8.3	7.44	7.3	13	9.6	11.7	4.4	9.20
Ga	15.5	16.2	15.2	16.3	16.4	15.9	13.6	13.6	14.0	14.7	14.7	14.12
Ba	717	901	709	765	799	778.2	573	589	594	445	462	530.6
Zr	151	179	144	177	177	165.6	106	113	135	139	105	106.6
Hf	4.4	5.1	4.4	5.3	5.0	4.84	3.2	3.6	4.0	3.9	3.5	3.64
La	31.0	35.7	30.6	35.2	36.6	33.82	21.0	30.4	61.1	38.1	26.5	35.42
Ce	60.6	68.2	58.6	67.7	72.0	65.42	37.9	54.6	100.6	65.2	48.2	61.30
Pr	7.0	7.9	6.9	7.8	8.2	7.56	4.0	5.6	10.4	7.1	5.6	6.54
Nd	26.1	30.3	25.4	29.4	31.4	28.52	13.7	19.3	31.3	23.8	19.8	21.58
Sm	5.0	5.5	5.1	5.5	6.1	5.44	2.6	3.1	4.3	3.8	3.6	3.48
Eu	1.07	1.32	0.99	1.13	1.22	1.146	0.61	0.63	0.69	0.62	0.59	0.63
Gd	4.37	4.79	4.22	4.76	5.76	4.78	2.42	2.74	3.11	3.40	3.27	2.99
Tb	0.70	0.69	0.64	0.73	0.99	0.75	0.41	0.45	0.44	0.47	0.55	0.46
Dy	3.68	3.77	3.48	4.00	5.43	4.07	2.61	2.72	2.64	2.95	3.27	2.24
Ho	0.68	0.66	0.64	0.74	1.09	0.76	0.54	0.54	0.53	0.61	0.69	0.58
Er	1.89	1.87	1.68	2.01	3.09	2.11	1.57	1.63	1.52	1.88	2.09	1.74
Tm	0.28	0.27	0.27	0.31	0.48	0.32	0.25	0.26	0.26	0.28	0.34	0.28
Yb	1.78	1.80	1.69	1.96	2.88	2.02	1.74	1.75	1.70	1.90	2.32	1.88
Lu	0.26	0.27	0.24	0.30	0.42	0.30	0.27	0.25	0.26	0.29	0.36	0.29
∑REE	144.41	163.04	140.45	161.54	175.66	157.016	89.62	123.97	218.85	150.4	117.18	140.0
Ti	2157.84	2397.60	2037.96	2217.78	2517.48	2277.72	1618.38	1738.26	1858.14	1918.08	1318.68	1690.31
Nb/Th	1.101	0.963	0.960	0.942	1.442	1.064	0.522	0.333	0.324	0.472	0.481	0.43
Nb/Y	0.6	0.65	0.67	0.62	0.47	0.59	0.47	0.44	0.60	0.59	0.48	0.52
Zr/Y	7.55	8.95	8.00	8.43	5.53	7.46	7.07	7.06	9.00	8.18	5.00	7.26

(*Continued*)

Table 2. (Continued).

	EK-1	EK-4	EK-6	EK-8	EK-25		EK-5	EK-10	EK-16	EK-18	EK-52	
Granitoid	M	M	M	M	M	Mean	G	G	G	G	G	Mean
Zr/Ti	0.07	0.07	0.07	0.08	0.07	0.07	0.07	0.07	0.07	0.07	0.08	0.07
La/Yb	17.42	19.83	18.11	17.96	12.71	16.74	12.07	17.37	35.94	20.05	11.42	19.37
$(La/Yb)_N$	12.49	14.23	12.99	12.88	9.12	12.01	8.66	12.46	25.78	14.38	8.19	13.89
$(La/Sm)_N$	4.00	4.19	3.87	4.13	3.87	4.01	5.21	6.33	9.17	6.47	4.75	6.39
$(Gd/Yb)_N$	2.03	2.20	2.07	2.01	1.65	1.96	1.15	1.30	1.51	1.48	1.17	1.32
$(Eu/Eu^*)_N$	0.7	0.78	0.87	0.67	0.63	0.73	0.74	0.66	0.57	0.53	0.53	0.61

	EK-19	EK-20	EK-22	EK-23	EK-24	EK-26	EK-31	EK-32	EK-28	EK-53	EK-27	EK-57		EK-9	EK-15
Granitoid	L	L	L	L	L	L	L	L	L	L	L	L	Mean	E	E
SiO_2 (wt%)	77.0	77.1	76.0	76.2	76.4	77.7	75.4	76.5	77.0	76.2	76.1	76.6	76.52	56.5	64.0
TiO_2	0.05	0.05	0.04	0.05	0.04	0.07	0.08	0.07	0.02	0.03	0.03	0.03	0.05	0.79	0.46
Al_2O_3	12.3	12.6	12.8	12.6	12.7	12.2	12.9	12.7	12.5	12.8	12.9	12.6	12.63	16.1	15.0
Fe_2O_3	1.05	0.92	0.94	0.98	0.97	1.21	1.33	1.08	1.07	0.75	0.88	0.91	1.01	10.35	6.10
MnO	0.03	0.02	0.01	0.02	0.01	0.02	0.06	0.06	0.06	0.01	0.01	0.01	0.03	0.21	0.12
MgO	0.04	0.04	0.05	0.04	0.06	0.04	0.14	0.12	0.03	0.10	0.03	0.10	0.07	3.00	2.69
CaO	0.60	0.73	1.05	0.56	1.07	0.64	0.74	0.78	0.74	0.84	0.83	1.08	0.81	5.62	5.46
Na2O	3.45	3.44	2.81	3.48	2.88	3.25	3.41	3.44	3.57	2.50	3.31	2.99	3.21	2.80	2.97
K2O	4.64	4.70	5.25	4.98	5.10	4.94	5.08	4.90	4.66	6.07	5.10	4.90	5.03	2.06	1.98
P_2O_5	0.00	0.01	0.02	0.02	0.03	0.01	0.02	0.03	0.02	0.01	0.02	0.01	0.02	0.07	0.08
Cr_2O_3	0.05	0.02	0.02	0.04	0.05	0.02	0.04	0.02	0.03	0.05	0.02	0.04	0.03	0.01	0.01
LOI	0.80	0.40	1.00	0.90	0.60	-0.20	0.70	0.30	0.20	0.60	0.70	0.70	0.56	0.82	0.54
Sum	99.99	99.97	99.97	99.93	99.95	99.94	99.92	99.93	99.95	99.96	99.98	99.95	99.95	98.33	99.39
Rb (ppm)	376	339	209	444	198	398	400	385	305	234	263	209	313.33	170	128
Sr	6	10	24	9	26	7	29	28	5	35	20	30	19.08	105	143
Nb	13	20	14	40	6	34	22	22	5	2	10	10	16.50	10	8
Y	16	21	18	47	11	26	47	36	26	11	35	30	27.00	34	23
Cs	17.4	7.9	5.1	14.0	4.6	5.1	7.7	6.8	5.7	5.0	4.2	3.0	7.21	13.0	8.4
Ta	2.3	2.7	3.7	5.3	1.3	3.7	3.1	3.6	1.0	0.6	2.8	2.9	2.75	1.2	1.2
Sc	0.9	0.9	0.9	2.0	0.9	2.0	3.0	2.0	0.9	0.9	0.9	2.0	1.44	25.0	14.7
Pb	8.8	8.8	4.8	12.5	6.7	15.4	7.1	5.4	7.9	9.2	9.2	6.4	8.52	18.4	22.5
U	3.2	5.5	10.1	18.0	5.5	5.1	11.7	16.0	5.6	6.5	7.0	5.2	8.28	3.3	4.8
Th	18.1	32.9	26.8	34.8	30.9	32.8	33.9	34.3	45.2	33.4	28.8	25.7	31.47	4.7	11.6
Ni	7.2	5.2	4.3	4.8	8.4	3.1	5.8	6.7	6.4	6.1	5.6	8.2	5.98	3.7	13.7
Ga	10.7	11.7	11.5	13.8	11.4	12.5	12.8	12.9	12.5	10.9	12.4	12.3	12.12	18.3	14.6
Ba	6	5	13	21	16	13	128	109	9	44	17	49	35.83	214	305
Zr	28	47	24	82	43	68	75	82	85	61	69	57	60.08	35	50
Hf	1.5	2.3	1.5	4.4	2.3	3.0	3.0	3.2	4.5	2.8	3.9	3.2	2.97	1.74	2.91
La	8.3	8.8	8.8	11.5	7.7	11.5	19.3	18.6	8.5	17.4	13.2	17.1	12.56	10.3	11.3
Ce	23.3	19.6	22.1	27.0	24.6	25.4	38.9	37.5	17.9	39.1	26.8	32.1	27.86	27.9	29.5
Pr	2.2	2.4	2.4	3.4	2.0	3.0	4.2	4.1	2.2	3.9	2.9	3.9	3.05	4.2	4.0
Nd	8.2	8.9	8.4	12.8	7.0	10.6	14.9	14.5	7.7	13.0	9.7	13.0	10.73	17.8	16.0
Sm	2.0	2.2	1.9	3.8	1.5	2.9	3.9	3.5	1.8	2.4	2.4	3.1	2.62	4.4	3.4
Eu	0.11	0.16	0.17	0.11	0.17	0.09	0.16	0.17	0.06	0.23	0.12	0.14	0.14	0.85	0.76
Gd	1.86	2.40	2.04	4.37	1.37	3.09	4.51	3.91	1.96	1.87	2.63	3.28	2.77	5.28	3.81
Tb	0.40	0.49	0.43	1.00	0.25	0.67	1.00	0.83	0.42	0.30	0.61	0.64	0.59	0.92	0.64
Dy	2.40	3.08	2.63	6.44	1.52	4.25	6.34	5.15	2.96	1.75	4.27	4.28	3.76	5.51	3.79
Ho	0.53	0.71	0.66	1.50	0.35	0.94	1.49	1.14	0.78	0.37	1.04	0.93	0.87	1.23	0.83

(*Continued*)

Table 2. (Continued).

Granitoid	EK-19	EK-20	EK-22	EK-23	EK-24	EK-26	EK-31	EK-32	EK-28	EK-53	EK-27	EK-57		EK-9	EK-15
	L	L	L	L	L	L	L	L	L	L	L	L	Mean	E	E
Er	1.73	2.28	2.15	4.95	1.16	2.85	4.53	3.49	2.69	1.16	3.59	3.06	2.80	3.70	2.66
Tm	0.31	0.41	0.40	0.90	0.23	0.50	0.76	0.60	0.52	0.24	0.70	0.54	0.51	0.60	0.36
Yb	2.28	2.85	2.87	6.43	1.63	3.26	5.04	4.04	4.04	1.56	5.10	3.76	3.57	4.07	2.71
Lu	0.34	0.46	0.44	1.04	0.28	0.49	0.74	0.62	0.67	0.26	0.83	0.63	0.57	0.64	0.43
ΣREE	53.96	54.74	55.39	85.24	49.76	69.54	105.77	98.15	52.2	83.54	73.89	86.46	72.4	87.4	80.19
Ti	299.70	299.70	239.76	299.70	239.76	419.58	479.52	419.58	119.88	179.82	179.82	179.82	299.70	4735.25	2757.24
Nb/Th	0.72	0.61	0.52	1.15	0.19	1.04	0.65	0.64	0.11	0.06	0.35	0.39	0.52	2.13	0.69
Nb/Y	0.81	0.95	0.78	0.85	0.55	1.31	0.47	0.61	0.19	0.18	0.29	0.33	0.61	0.29	0.35
Zr/Y	1.75	2.24	1.33	1.74	3.91	2.62	1.60	2.28	3.27	5.55	1.97	1.90	2.23	1.03	2.17
Zr/Ti	0.09	0.16	0.10	0.27	0.18	0.16	0.16	0.20	0.71	0.34	0.38	0.32	0.20	0.01	0.02
La/Yb	3.64	3.09	3.07	1.79	4.72	3.53	3.83	4.60	2.10	11.15	2.59	4.55	3.52	2.53	4.17
$(La/Yb)_N$	2.61	2.21	2.20	1.28	3.39	2.53	2.75	3.30	1.51	8.00	1.86	3.26	2.52	1.82	2.99
$(La/Sm)_N$	2.68	2.58	2.99	1.95	3.31	2.56	3.19	3.43	3.05	4.68	3.55	3.56	3.09	1.51	2.15
$(Gd/Yb)_N$	0.67	0.70	0.59	0.56	0.70	0.78	0.74	0.80	0.40	0.99	0.43	0.72	0.64	1.07	1.16
$(Eu/Eu^*)_N$	0.17	0.21	0.26	0.08	0.36	0.09	0.11	0.14	0.09	0.33	0.15	0.13	0.17	0.54	0.64

and 644°C–734°C (average 704°C) for the leucogranites. Their apatite saturation temperatures vary from 763°C to 883°C (average 850°C) for the granodiorites, from 790°C to 947°C for the microgranites (880°C), and from 769°C to 856°C (average 809°C) for the leucogranites. The zircon and apatite saturation temperatures imply that the magma temperatures are in range of 758°C and 850°C for the granodiorites, in range of 797°C–880°C for the microgranites, and in range of 704°C–809°C for the leucogranites. The temperature ranges increase from the leucogranite, granodiorites to microgranites (Table 5). Lower temperatures estimated by Toksoy-Köksal (2016) infer recrystallisation at a late stage during slow cooling. Also, the values calculated from the zircon and apatite saturation methods are reliable, reflecting crystallisation temperatures.

7. Discussion

Intrusive rocks in the Ekecikdağ area display different granitoid types, which evolved in a short period in the Late Cretaceous. U-Pb crystallisation ages of the granodiorites and the microgranites were determined as 84.52 ± 0.93 Ma and 80.7 ± 1.6 Ma, respectively, whereas the age of the leucogranites is suggested as 80 Ma relative age, based on the field relations and considering the $^{206}Pb/^{238}U$ and Rb-Sr ages. These granitoids not only show distinct ages but also differ from each other in their field, petrographical, mineralogical, whole-rock element and even isotopic geochemical characteristics. In spite of the variable petrological characteristics, they are combined to form an igneous association in a particular geodynamic setting. The petrological investigation of the EIA using new geochronological and isotopic data is crucially important as a contribution to the geodynamic evolution of Central Anatolia.

There are different views about the evolution of the CACC granitoids, which have been discussed in several studies. Basically, one view suggests that the CACC granitoids were generated in collisional to post-collisional systems (Göncüoğlu et al., 1991, 1992, 1993, 1997a,1997b; Göncüoğlu & Türeli, 1994; Erler & Göncüoğlu, 1996; Yalınız et al., 1999; Boztuğ, 1998, 2000; Boztuğ et al., 2007a; 2007b; Boztuğ et al., 2007c; 2008, 2009; Düzgören-Aydın et al., 2001; Köksal et al., 2004, 2012, 2013; Tatar & Boztuğ, 1998; Delibaş et al., 2011; Toksoy-Köksal, 2016; Hinsbergen et al., 2016). According to this view, the Alpine orogenesis resulted in closure of the İzmir-Ankara-Erzincan branch of the Neotethyan Ocean (e.g. Boztuğ, 1998, 2000; Düzgören-Aydın et al., 2001; Erler & Göncüoğlu, 1996; Göncüoğlu et al., 1993, 1992, 1997a, 1997b; Göncüoğlu et al., 1991; Göncüoğlu & Türeli, 1994; Yalınız et al., 1999). During the closure, ensimatic island arc was developed in a supra-subduction zone. With further closure, all the

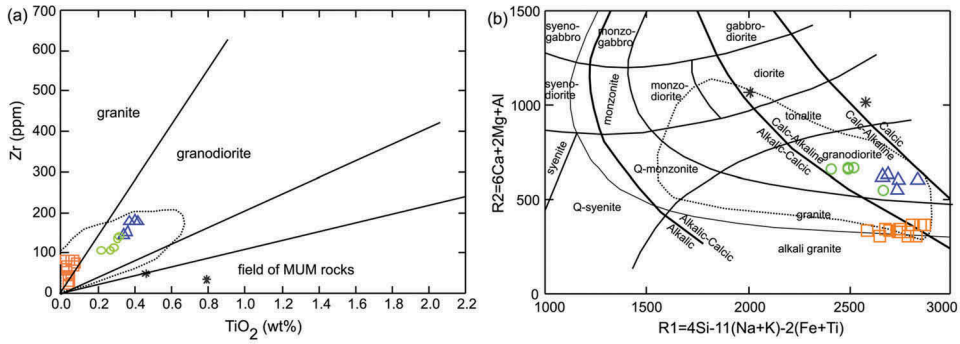

Figure 11. Geochemical plots of the granitoids on (a) the Zr versus TiO_2 classification diagram (Winchester & Floyd, 1977) and (b) R2 versus R1 diagram (De La Roche et al., 1980) (symbols and explanation of the area defined by dashed line are given in Figure 10).

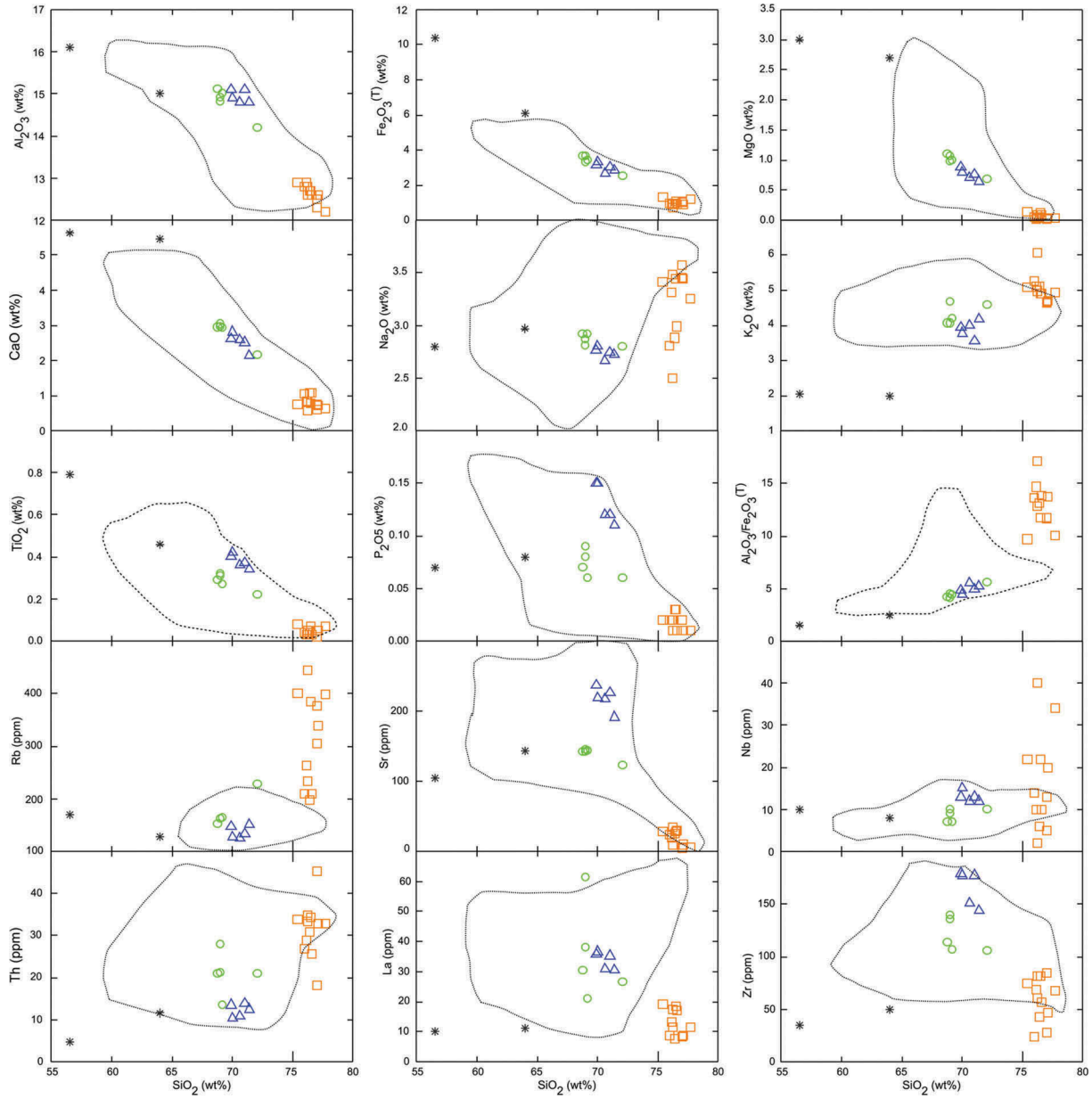

Figure 12. Bivariate plots of major oxides and trace elements against SiO_2 (symbols and explanation of the area defined by dashed line are given in Figure 10).

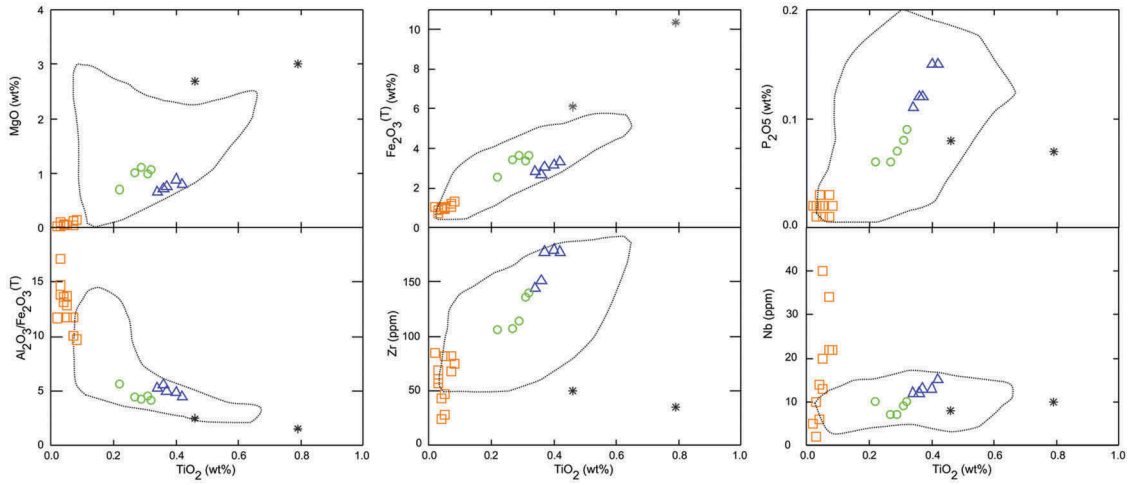

Figure 13. Bivariate plots against TiO_2 (symbols and explanation of the area defined by dashed line are given in Figure 10).

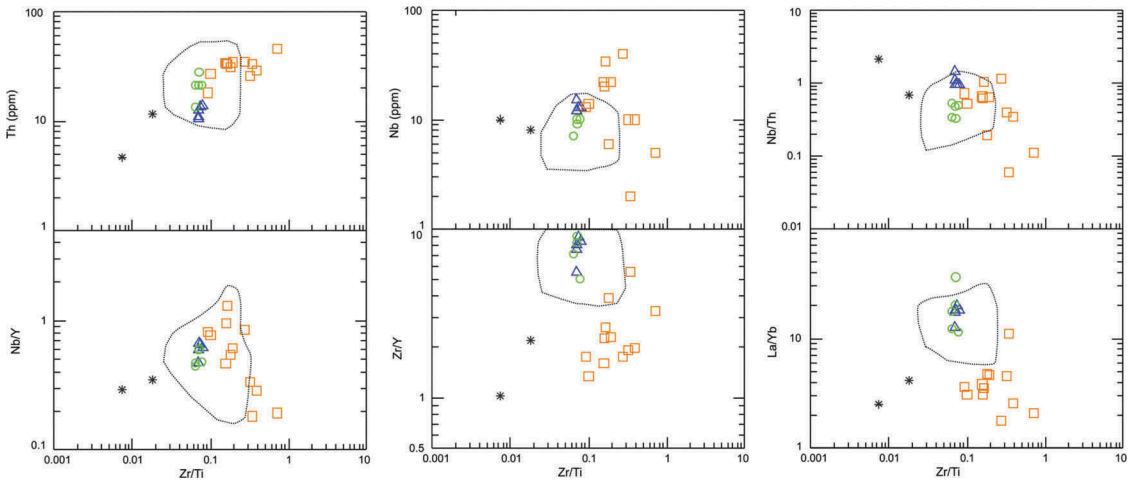

Figure 14. Bivariate plots against Zr/Ti (symbols and explanation of the area defined by dashed line are given in Figure 10).

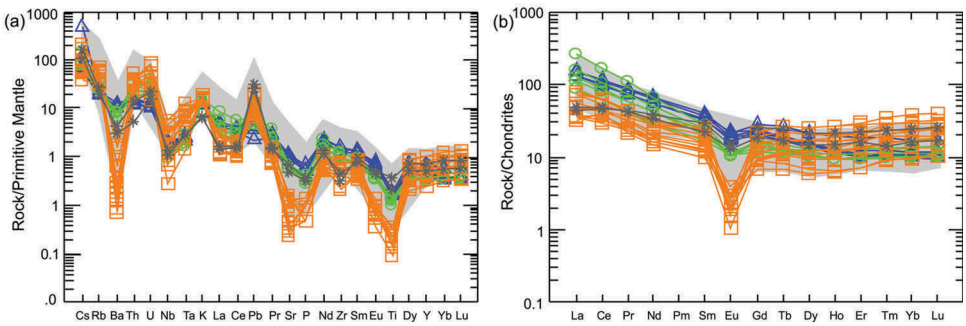

Figure 15. (a) Primitive mantle normalised trace element spider diagram and (b) chondrite normalised REE pattern (normalising values from Sun & Mcdonough, 1989) (symbols are given in Figure 10) (grey-colored area represent the Ağaçören granitoids (see Figure 10 for references).

oceanic rocks represented by MORB, OIB and island arc as well as accretion prism materials, were obducted onto the passive margin of the Tauride-Anatolide microplate during the Middle Cretaceous (e.g. Floyd, Göncüoğlu, Winchester, & Yalınız, 2000; Yalınız, Göncüoğlu, & Özkan-Altıner, 2000; Toksoy-Köksal et al., 2009; see Figure 9 in Köksal et al., 2012). Obduction of the ophiolitic-nappes gave way to crustal thickening at the passive CACC margin and caused medium-high temperature regional metamorphism followed by formation of the collisional to post-collisional granitic rocks of Central Anatolia in the Late Cretaceous (e.g. Göncüoğlu et al., 1991, 1992, 1993, 1997a,b; Göncüoğlu & Türeli, 1994; Erler & Göncüoğlu, 1996; Yalınız et al.,

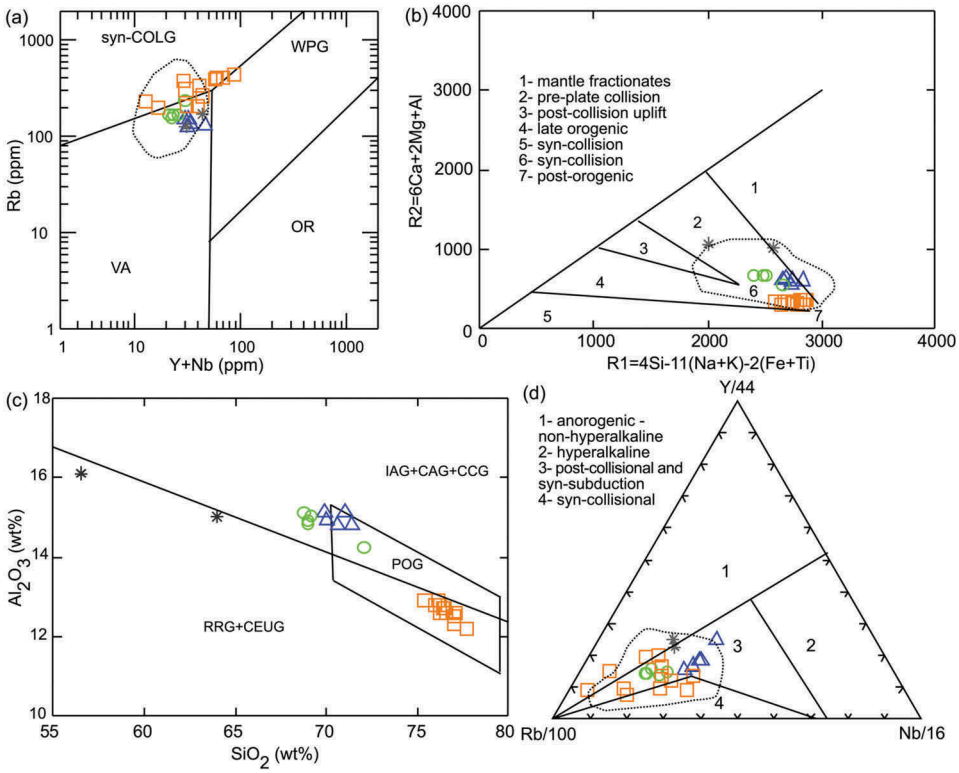

Figure 16. Geochemical plots of the granitoids on the tectonodiscrimination diagrams (a) Rb vs. Y+ Nb (syn-coln: syn-collisional granitoids, WPG: within plate granites, VAG: volcanic arc granites, ORG: orogenic granites, Pearce et al., 1984), (b) R2 vs. R1 (Batchelor & Bowden, 1985) and (c) Al_2O_3 vs. SiO_2 (RRG+CEUG: rift related granitoids and continental epiorogenic uplift granitoids, POG: post-orogenic granitois, IAG+CAG+CCG: island arc granitoids, continental arc granitoids and continental collisional granite, Maniar & Piccoli, 1989), (d) Y/44–Rb/100–Nb/16 (Thiéblemont & Cabanis, 1990) (Symbols and explanation of the area defined by dashed line are given in Figure 10).

Table 3. Sr and Nd isotope data from the Ekecikdag Granitoids (Granitoid types: M-microgranite, G: granodiorite, L: leucogranite).

Sample no.	Granite type	$^{87}Sr/^{86}Sr$	Rb (ppm)	Sr (ppm)	$^{87}Sr/^{86}Sr_{(T)}$ (1)	$^{143}Nd/^{144}Nd$	Nd (ppm)	Sm (ppm)	$^{143}Nd/^{144}Nd_{(T)}$ (1)	$\varepsilon Nd_{(T)}$	T_{DM}
EK-1	M	0.715488 ± 6	126.1	217.1	0.713529	0.512154 ± 3	26.1	5.04	0.512092	−8.62	1.59
EK-4	M	0.715537 ± 5	148.4	237.4	0.713429	0.512144 ± 3	30.3	5.53	0.512085	−8.75	1.60
EK-6	M	0.715970 ± 5	152.3	190.9	0.713279	0.512150 ± 3	25.4	5.05	0.512086	−8.73	1.60
EK-8	M	0.715509 ± 5	133.3	226.1	0.713520	0.512146 ± 4	29.4	5.49	0.512086	−8.73	1.60
EK-25	M	0.715693 ± 5	126.5	218.9	0.713744	0.512159 ± 3	31.4	6.12	0.512097	−8.53	1.58
EK-5	G	0.713539 ± 6	163.7	142.6	0.709762	0.512243 ± 12	13.7	2.63	0.512179	−6.84	1.44
EK-10	G	0.713055 ± 5	151.5	142.2	0.709538	0.512237 ± 3	19.3	3.11	0.512183	−6.76	1.44
EK-16	G	0.715624 ± 9	163.3	144.9	0.711916	0.512179 ± 3	31.3	4.26	0.512134	−7.73	1.52
EK-18	G	0.715320 ± 16	162.9	142.2	0.711577	0.512188 ± 3	23.8	3.81	0.512135	−7.71	1.52
EK-52	G	0.718661 ± 10	227.1	121.6	0.712353	0.512175 ± 3	19.8	3.61	0.512114	−8.11	1.55
EK-31	L	0.751671 ± 5	400.0	29.0	0.707419	0.512302 ± 3	14.9	3.87	0.512220	−6.15	1.39
EK-32	L	0.752031 ± 5	384.8	27.5	0.707138	0.512306 ± 3	14.5	3.47	0.512230	−5.95	1.37
EK-27	L	0.751514 ± 5	262.6	20.0	0.709389	0.512221 ± 4	9.7	2.40	0.512143	−7.66	1.51
EK-57	L	0.731832 ± 11	209.1	30.4	0.709765	0.512271 ± 3	13.0	3.08	0.512196	−6.62	1.42

(1) t = 81 Ma (for microgranite); 84.5 Ma (for granodiorite); 80 Ma (for leucogranite).

1999; Boztuğ, 1998, 2000; Düzgören-Aydın et al., 2001). The other view, on the other hand, states that the Inner Tauride ocean, separating the Tauride carbonate platform from the Anatolide block, was subducted beneath the CACC and Andean-type style magmatic arc granitoids were derived (Deniz & Kadıoğlu, 2016; Görür et al., 1984; Kadıoğlu et al., 2003; Okay et al., 1996; Şengör & Yılmaz, 1981).

Kadıoğlu et al. (2003) interpreted the granitoids in the Ağaçören Intrusive Suite (AIS), which seems to be the northwest continuation of the EIA, as a product of a magmatic arc evolved at the active margin of the western edge of the CACC. Moreover, Kadıoğlu et al. (2006) determined the $^{40}Ar/^{39}Ar$ age of the AIS granitoids as 77.7 ± 0.3 Ma and suggested that partial melts were formed by the injection of metasomatized upper mantle melts into the continental crust. These partial melts result in the interaction of mantle- and crustal-derived magmas accompanied by the combined assimilation–fractional crystallisation, mixing and mingling processes and generated the calc-alkaline magmas as sources of these

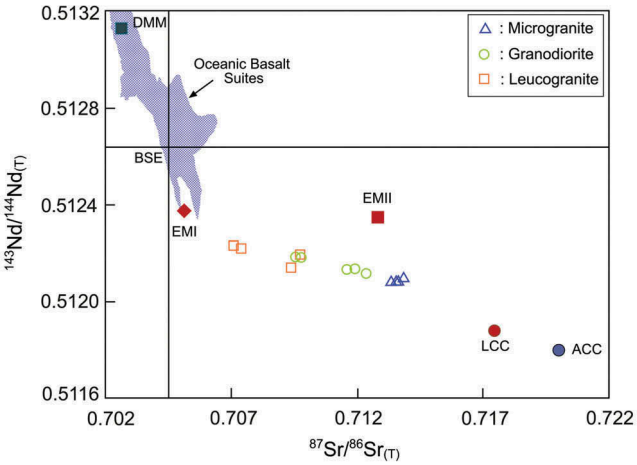

Figure 17. Initial $^{143}Nd/^{144}Nd$ vs. $^{87}Sr/^{86}Sr$ diagram of the Ekecikdağ granitoids. BSE: Bulk Silicate Earth (Workman & Hart, 2005), EM I: Enriched Mantle I (Richardson, Erlank, Duncan, & Reid, 1982), Enriched Mantle II (Workman et al., 2004), DMM: Depleted MORB Mantle (Workman & Hart, 2005), ACC: Average Continental Crust (Hofmann, 1997), LC: Lower Crust (Villaseca, Downes, Pin, & Barbero, 1999), Oceanic Basalt Suites (Zindler & Hart, 1986).

granitoids (Kadıoğlu et al., 2006). Köksal et al. (2012), on the other hand, presented LA-ICP-MS U-Pb zircon age data yielding an age range from 84 to 74 Ma for the AIS granitoids and described them as collisional to post-collisional formed due to crustal thickening after obduction of the ophiolitic rocks onto the TAP. Therefore, there is no consensus on petrogenesis of the granitoids in the Ağaçören area. For that reason, the previous geochemical data from the AIS granitoids are compared with those of the EIA granitoids to better understand the nature of the granitoids within that part of the CACC. The whole-rock element geochemical data compiled from Kadıoğlu et al. (2003), (2006) and Köksal et al. (2012) for the granitoids from the Ağaçören area well compare with data of the EIA granitoids (Figure 10–16). Moreover, the Sr-Nd isotope data from the Ağaçören granitoids ($[^{87}Sr/^{86}Sr]_T$: 0.709143 to 0.715191; εNd: −6.48 to −8.84) (Köksal et al., 2012) are also comparable to those of the EIA granitoids.

Tectonic discrimination diagrams of the EIA granitoids reveal their collisional to post-collisional character (Figure 16). This is in accordance with the description of the other CACC granitoids with collisional to post-collisional nature (e.g. Boztuğ, 1998, 2000; Göncüoğlu & Türeli, 1994; Köksal et al., 2012, 2013).

Although all three rock types show sub-alkaline and high-K calc-alkaline features, their alumina indexes are different (Toksoy-Köksal, 2016). The mafic enclave-rich granodiorites have hornblende and plagioclase as essential phases and titanite as an accessory mineral. The granitoids are metaluminous to peraluminous, and reveal an I-type granitoid nature (granitoid formed by partial melting of metamagmatic crust, e.g. Chappell, White, & Wyborne, 1987). The microgranites and the leucogranites with two micas (biotite + primary muscovite), in contrast, are peraluminous and imply that these rocks are S-type granitoids not bearing hornblende (granitoids formed from sedimentary protoliths; e.g. Chappell & White, 1974). Both microgranites and leucogranites are peraluminous, whereas the leucogranites display lower ACNK values due to the presence of orthoclase and the albitic composition of plagioclase. EPMA analyses of biotites support the peraluminous character of the microgranites (Toksoy-Köksal, 2016).

SiO_2 contents of the granodiorites and the microgranites are similar in range, but lower than the leucogranites. The relation of the granodiorites and the microgranites to the leucogranites due to decreasing Al_2O_3, $Fe_2O_3^{(T)}$, MgO, CaO contents but increasing SiO_2 may infer fractional crystallisation (Figure 12). However, on the diagrams of TiO_2 against $Fe_2O_3^{(T)}$/Al_2O_3, $Fe_2O_3^{(T)}$, MgO and P_2O_5, there are no continuous trends observed through the granodiorites, the microgranites and the leucogranites representing a fractional crystallisation (Figure 13). Trends of Zr against SiO_2 and TiO_2 show that the leucogranites are separate from the granodiorites and the microgranites (Figure 12, 13). Moreover, the granodiorites and the microgranites, with similar Zr/Ti values, display markedly different patterns to the leucogranites on the Zr/Ti against Th, Nb, Nb/Th, Nb/Y, Zr/Y, La/Yb diagrams (Figure 14). The overlapping plots on the diagrams of SiO_2 against $Al_2O_3/Fe_2O_3^{(T)}$ may imply that the granodiorites and the microgranites have a cogenetic origin than the leucogranites (Figure 12). The granodiorites and the microgranites have also overlapping values of Nb/Y, Zr/Y, La/Yb that may infer derivation/evolution from the same source and then fractionation (Figure 14). However, the granodiorites with lower Nb and higher Th have a lower Nb/Th ratio that separates the granodiorites from the microgranite. Moreover, the plots of TiO_2 against

Table 4. LA-MC-ICP-MS Lu-Hf isotope data and corresponding LA-ICP-MS $^{206}Pb/^{238}U$ ages of zircons from the EIA granitoids.

Analyse nr:	$^{176}Yb/^{177}Hf$ [a]	±2 σ	$^{176}Lu/^{177}Hf$ [a]	±2 σ	$^{178}Hf/^{177}Hf$	$^{180}Hf/^{177}Hf$	Sig_{Hf} [b] (V)	$^{176}Hf/^{177}Hf$	±2 σ	$^{176}Hf/^{177}Hf_{(t)}$	ƐHf(t) [c]	±2 σ	T_{DM2} [d] (Ga)	Age [e] (Ma)	±2 σ
L-1	0.0754	32	0.00213	10	1.46718	1.88677	22	0.282628	20	0.282624	−3.4	0.7	1.19	84	3
L-2	0.0388	37	0.00112	11	1.46718	1.88678	22	0.282685	15	0.282683	−1.3	0.5	1.08	84	3
L-3	0.0503	7	0.00147	3	1.46719	1.88678	20	0.282620	19	0.282618	−3.7	0.7	1.20	82	3
M-1	0.0325	16	0.00092	6	1.46730	1.88690	25	0.282143	19	0.282133	−9.0	0.7	1.93	618	24
M-2	0.0234	37	0.00058	8	1.46718	1.88696	16	0.282340	18	0.282332	−0.2	0.6	1.51	694	24
M-3	0.0437	10	0.00123	3	1.46723	1.88692	20	0.282579	16	0.282577	−5.0	0.6	1.28	86	3
M-4	0.0350	8	0.00097	2	1.46717	1.88671	20	0.282505	17	0.282503	−7.7	0.6	1.43	81	3
M-5	0.0340	13	0.00095	4	1.46728	1.88699	18	0.282505	17	0.282504	−7.6	0.6	1.42	85	3
M-6	0.0448	24	0.00123	5	1.46719	1.88673	21	0.281730	16	0.281706	−15.4	0.6	2.59	1008	16
M-7	0.0406	12	0.00124	3	1.46726	1.88699	19	0.282576	19	0.282574	−5.3	0.7	1.29	79	3
M-8	0.0356	31	0.00100	9	1.46715	1.88675	21	0.282515	16	0.282513	−7.3	0.6	1.40	82	3
M-9	0.0499	38	0.00146	11	1.46720	1.88679	19	0.282532	20	0.282530	−6.8	0.7	1.37	79	3
M-10	0.0403	14	0.00112	4	1.46728	1.88700	19	0.282501	18	0.282500	−7.8	0.6	1.43	83	3
M-11	0.0390	11	0.00109	3	1.46722	1.88694	18	0.282192	21	0.282172	0.2	0.7	1.71	968	33
M-12	0.0388	18	0.00119	5	1.46721	1.88691	18	0.282540	19	0.282539	−6.5	0.7	1.36	80	2
M-13	0.0501	20	0.00153	6	1.46734	1.88704	19	0.282572	19	0.282570	−5.4	0.7	1.30	79	2
G-1	0.0522	10	0.00144	3	1.46728	1.88700	19	0.282608	18	0.282606	−4.1	0.7	1.23	82	3
G-2	0.0359	4	0.00103	1	1.46726	1.88691	18	0.282563	19	0.282561	−5.6	0.7	1.31	85	2
G-3	0.0400	29	0.00097	7	1.46720	1.88691	17	0.282257	18	0.282246	−5.5	0.7	1.72	595	18
G-4	0.0420	31	0.00103	8	1.46726	1.88681	17	0.282282	19	0.282269	−3.2	0.7	1.65	663	27
G-5	0.0440	45	0.00116	12	1.46723	1.88681	16	0.281863	23	0.281846	−16.1	0.8	2.43	755	25
G-6	0.0285	15	0.00084	3	1.46720	1.88685	17	0.282574	18	0.282572	−5.2	0.6	1.29	86	2
G-7	0.0414	9	0.00108	2	1.46728	1.88704	14	0.282516	19	0.282515	−7.2	0.7	1.40	85	3
G-8	0.0422	20	0.00128	9	1.46735	1.88693	17	0.282516	19	0.282514	−7.2	0.7	1.40	87	3
G-9	0.0315	8	0.00090	2.56	1.46719	1.88686	18	0.282546	16	0.282545	−6.2	0.6	1.34	86	3
GJ-1 [f]	0.01036	94	0.000307	8	1.46721	1.88685	19	0.282005	13	0.282002	−13.8	0.5	2.19	609	9

(a) $^{176}Yb/^{177}Hf = (^{176}Yb/^{177}Hf)_{true} \times (^{173}Yb/^{177}Hf)_{meas} \times (M_{176(Yb)}/M_{173})^{ß(Yb)}/(M_{176(Yb)}/M_{177})^{ß(Yb)}$ (Hf). $^{176}Lu/^{177}Hf$ values were calculated in a similar way by using the measured $^{175}Lu/^{177}Hf$ and the $ß_{Yb}$. The effect of the inter-element fractionation on the Lu/Hf was estimated to be 4–6 %. (b) Mean Hf signal in volt. (c) calculated using a decay constant of 1.865×10^{-10} (Scherer et al. 2001), a CHUR $^{176}Lu/^{177}Lu$ and $^{176}Hf/^{177}Hf$ ratio of 0.0332 and 0.282772, and the ages obtained by LA-ICP-MS. (d) Two-stage model age using the measured $^{176}Lu/^{177}Lu$ of each spot (first stage = age of zircon), a value of 0.0113 for the average continental crust (second stage), and a depleted mantle $^{176}Lu/^{177}Lu$ and $^{176}Hf/^{177}Hf$ of 0.0384 and 0.28325, respectively. (e) U-Pb apparent zircon ages (source: Table 3). (f) Mean ± 2σ standard deviation of 11 spot analyses of GJ-1 reference zircon.

Table 5. Zircon and apatite saturation temperatures from the whole rock geochemical analyses.

	Zircon saturation temperature (°C)	Apatite saturation temperature (°C)
Microgranites		
EK1	788	790
EK4	802	801
EK6	786	928
EK8	808	933
EK25	780	947
Average	797	880
Granodiorites		
EK5	750	763
EK10	755	857
EK16	764	871
EK18	770	883
EK52	751	876
Average	758	850
Leucogranites		
EK19	656	777
EK20	691	778
EK22	644	819
EK23	731	821
EK24	683	856
EK26	716	783
EK31	723	814
EK32	731	856
EK28	734	828
EK53	706	769
EK27	722	820
EK57	704	793
Average	704	809
Mafic enclaves		
EK9	652	709
EK15	681	817
Average	667	763

Al_2O_3/TiO_2, $Fe_2O_3^{(T)}/Al_2O_3$, $Fe_2O_3^{(T)}$, MgO (Figure 13), and plots of SiO_2 against TiO_2 and P_2O_5 (Figure 12) give two almost parallel trends for the granodiorites and the microgranites, which opposes their cogenetic origin (Figure 12). Moreover, no magmatic differentiation trends are observed from the granodiorites and the microgranites linked to the leucogranites on the SiO_2 versus Rb, Sr, Nb, Th, Zr and La variation diagrams (Figure 12). Bivariate plots clearly display a good separation of the Ekecikdağ granitoids from each other that infers distinct genetic relations. Moreover, mineral-based petrological interpretations by Toksoy-Köksal (2016) strongly oppose a cogenetic relationships of the granitoids, especially as fractionation of the microgranite from the granodioritic magma. This assumption is supported by the crystallisation temperature of the microgranites calculated from zircon and apatite saturation formulations that is higher than the granodiorites. This means that the microgranites were not fractionated from the granodioritic melt.

Moreover, there are some whole-rock elemental and isotopic inputs that oppose their cogenetic character. Although all the granitoids have well-characterised positive anomalies in Th, La, Ce, Nd, Sm, U, K, Pb and negative anomalies in Nb, Zr, Eu, Ti, flat MREE and HREE on chondrite and primitive mantle normalised multi-element diagrams (Figure 15), the microgranites are enriched in Ba, Sr, P but depleted in Th and U compared to the granodiorites, even though similar enrichment and depletion levels are observed for both rock types. Furthermore, the leucogranites differ from the granodiorites and the microgranites by pronounced enrichment of Th, U and HREE, and depletion of Sr, P, Eu and Ti and LREE (Figure 15).

To clarify and understand genetic relationships of the rocks, the very incompatible elements (VICE: Th, U, Nb, Zr, Hf, Ti, Y) and moderately incompatible elements (MICE) are used in this study. Because VICE profoundly fractionate in melt residue but fractionate much less in the melt, they therefore preserve the same ratios as in the original source (Anderson, 2007; Hofmann, 2003), thus their ratios can reflect heterogeneity in the source. Moreover, use of moderately incompatible elements (MICE) relative to VICE may also reveal source heterogeneity (Hofmann, 2003; Hofmann & Jochum, 1996). In this study, VICE/MICE ratios (Nb/Yb) are plotted against Zr/Ti, Ti/Y, Nb/Th, La/Yb and ƐNd to throw light on source relations (Figure 19). The pronounced distinct plots on the Nb/Yb against Zr/Ti, Ti/Y and La/Yb and ƐNd diagrams infer that the source difference among the rock types are clear (Figure 19). The higher Zr/Ti and ƐNd values with lower Ti/Y and La/Yb of the leucogranites shows immediately that its source is different from both the granodiorites and the microgranites. The microgranites and the granodiorites have overlapping

Zr/Ti, Ti/Y and La/Yb (Figure 19), while the ℰNd of the granodiorites is higher than the microgranites but lower than the leucogranites. Moreover, where VICE/MICE ratios are plotted against $^{143}Nd/^{144}Nd$ (Figure 19) the leucogranites have higher Zr/Ti but lower Ti/Y, La/Yb, and low to moderate Nb/Th ratios against $^{143}Nd/^{144}Nd$, which infer that they have a significantly different source from the granodiorites and the microgranites (Figure 19). Nb/Th and ℰNd of the granodiorites overlap with the leucogranites but are different from the microgranites. Thus the microgranites might have a different source from the granodiorites.

The pronounced negative Eu anomalies ($(Eu/Eu^*)_N$) in the leucogranites (0.09–0.36), the microgranites (0.63–0.78) and the granodiorites (0.53–0.74) reflect fractional crystallisation of plagioclase. $(La/Yb)_N$, $(La/Sm)_N$ and $(Gd/Yb)_N$ ratios change from 8.19 to 25.78 (average = 13.89), 4.75 to 9.17 (average = 6.39), 1.15 to 1.51 (average = 1.32) for the granodiorites, 9.12 to 14.23 (average = 12.01), 3.87 to 4.19 (average = 4.01), 1.65 to 2.20 (average = 1.96) for the microgranites, 1.28 to 8.0 (average = 2.52), 1.95 to 4.68 (average = 3.09), 0.40 to 0.99 (average = 0.64) for the leucogranites, respectively. High $(La/Yb)_N$ ratios for the granodiorites and the microgranites infer high fractionation of REE and the presence of garnet (Hauri, Wagner, & Grove, 1994; Petermann, Hirschmann, Hametner, Gunther, & Schmidt, 2003) and/or hornblende (Reichardt & Weinberg, 2012; Tiepolo & Tribuzio, 2008) in the source. Thus, the magma source could be garnet lherzolite or a meta-magmatic crustal source with garnet and hornblende (Toksoy-Köksal, 2016).

Mineral based petrological evidence infers that the S-type microgranites and leucogranites were derived by partial melting of a meta-sedimentary crustal source (Figure 18 in Toksoy-Köksal, 2016). In the origin of the I-type hybrid granodiorite, however, mixing of mantle and meta-magmatic and meta-sedimetary crust derived magmas might have played a role (Toksoy-Köksal, 2016). The I-type character of the granodiorites may reveal partial melting of a meta-magmatic crustal source (e.g. Chappell et al., 1987) while the S-type features of the microgranites and the leucogranites may reflect partial melting of a meta-

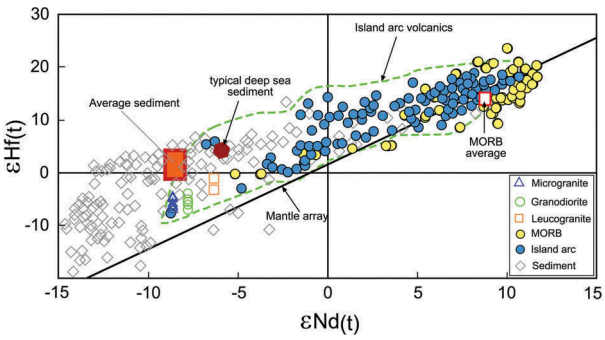

Figure 18. $\varepsilon Hf_{(t)}$ vs. $\varepsilon Nd_{(t)}$ plots of the EIA granitoids. The compared data are from Chauvel et al. (2008).

sedimentary crustal source (Chappell & White, 1974). However, evolution of all the data explains that it is too simple to classify the Ekecikdağ granitoids as S- and I-type (Toksoy-Köksal, 2016). Crustal contribution is signficant in the origin of the I-type granodiorites while a mantle contribution is present in the source of the mainly S-type leucogranites and microgranites. Therefore, heterogeneous sources derived from both mantle and crust (Chen, Xu, Chen, & Yu, 2016; Gray, 1984; Keay, Collins, & Mcculloch, 1997) are present in the protolith of the Ekecikdağ granitoids. Studies suggest mantle-derived magma in the origin of the S-type granitoids (e.g. Maas, Kamenetsky, Nicholls, & Steele, 2001), and reworking of crustal sedimentary material with mantle-like source (e.g. Kemp et al., 2007). A mixture of crustal rocks, including felsic-intermediate magmatic, metamorphic and sedimentary rocks may contribute to the source of the I-type granitic rocks (Chen et al., 2016). Hence a higher contribution from a mantle and/or meta-magmatic crustal source in origin of the Ekecikdağ granodiorites is possible. When these data collectively evaluated, the classical S-type and I-type classification does not seem to accurately reflect the petrogenesis of the Ekecikdağ granitoids. Because in the granodiorites with mainly I-type characteristics there is a significant crustal contribution, while in the S-type leucogranites and microgranites there is a mantle contribution. For this reason, as suggested by some authors like Gray (1984) and Keay et al. (1997) both S-, and I-type Ekecikdağ granitoids should have been derived from heterogenous source including mantle and crustal components. This is the case already inferred by some other studies disclosing S-type granitoids with mantle contribution (e.g. Maas et al., 2001) or I-type granitoids formed by reworking of sedimentary material (e.g. Kemp et al., 2007). Oxygen and sulphur isotope geochemistry displays a significant crustal source signature in the genesis of post-collisional granitoids in Central Anatolia (Boztuğ & Arehart, 2007). As a result, granitoids in the Ekecikdağ region can be assessed mainly as crustal granitoids having a mantle contribution.

Zircon Lu-Hf analyses reveal the robust petrogenetic nature of the host granitoids. The narrow range of initial $^{176}Hf/^{177}Hf$ ratios of Late Cretaceous analyses (i.e. 0.282500–0.282683) and $\varepsilon Hf_{(t)}$ values (i.e. −1.3 to −7.8) indicate no evidence for juvenile Cretaceous input. Moreover, these initial zircon Hf-isotope data indicate that the Ekecikdağ granitoids were not derived from melting of juvenile crust formed from depleted mantle since $\varepsilon Hf_{(t)}$ values are below zero and so not typical of a mantle source (e.g. Amelin, Lee, Halliday, & Pidgeon, 1999). The Ağaçören granitoids with zircon $\varepsilon Hf_{(t)}$ data ranging from −4.1 to −8.8 (Köksal et al., 2012) are comparable with zircon $\varepsilon Hf_{(t)}$ data, which correspond to Late Cretaceous, of

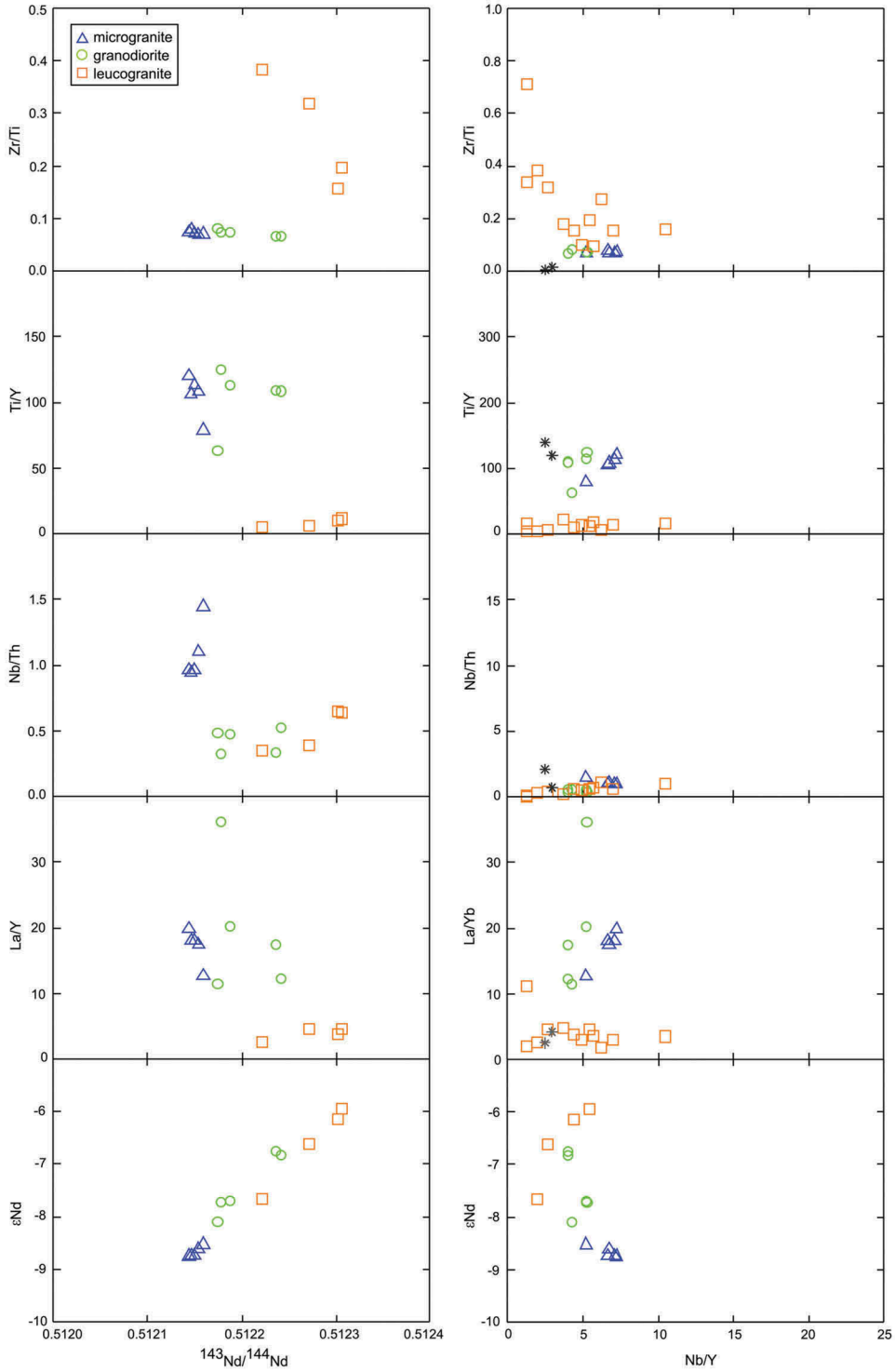

Figure 19. Bivariate plots of VICE/MICE ratios against $^{143}Nd/^{144}Nd$ and Nb/Y (symbols are given in Figure 10).

the Ekecikdağ granitoids. The unradiogenic Hf-isotope character of the zircons from the Ekecikdağ granitoids, along with the unradiogenic Neodymium whole-rock isotope data, away from the MORB and island arc volcanics sources, even below the typical deep sea sediment data, and close to the average sediment data, also infer a crust dominated source (Figure 18) (e.g. Chauvel, Lewin, Carpentier, Arndt, & Marini, 2008). Whole-rock Sr-Nd isotope data also support enriched sources with significant crustal contribution (Figure 17). The larger range of initial $^{176}Hf/^{177}Hf$ ratios (i.e. 0.281706–0.282683) and $\varepsilon Hf_{(t)}$ values (i.e. −16.1 to +0.2) corresponding to older ages (Table 4), contrariwise, indicates heterogeneity of the older sources. Zircon Lu-Hf isotope data consequently indicate traces of reworked crust in the petrogenesis of the Ekecikdağ granitoids. This phenomenon is also suggested for the Ağaçören granitoids located to the NW of the study area (e.g. Köksal et al., 2012). Therefore, it is suggested that the Ağaçören Intrusive Suite comprising granitoids, which are contemporaneous and show similarities in geochemical data

including whole-rock Sr-Nd and zircon Lu-Hf isotopes with the EIA granitoids, is likely to be have the same petrogenetical and geodynamical characteristics with the Ekecikdağ Intrusive Association.

In Central Anatolia, voluminous granites intrude basement metamorphic rocks and ophiolitic units. Schistose and gneissose meta-sedimentary rocks were formed at high temperature – medium pressure (maximum 700–770°C/6–8 kbar) upper amphibolite facies conditions at a maximum depth of 20–26 km (Lefebvre, Peters, Wehrens, Brouwer, & van Roermund, 2015; Whitney, Teyssier, Dilek, & Fayon, 2001) before 84.1 ± 0.8 Ma (Whitney & Hamilton, 2004). Retrograde metamorphism to greenschist facies took place at low pressure (3–4 kbar) and medium to high temperature (550–700°C) (Lefebvre et al., 2015; Whitney et al., 2001; Whitney, Teyssier, Fayon, Hamilton, & Heizler, 2003). S-type granitic intrusions accompanied the retrograde metamorphism due to pressure decrease (Lefebvre, Barnhoorn, van Hinsbergen, Kaymakci, & Vissers, 2011; Lefebvre et al., 2015; Whitney et al., 2001, 2003). These granitic intrusions were derived from partial melting of crustal metasedimentary rocks at high temperature and/or decrease of pressure (<12 km) but melting was not long lasting (Whitney et al., 2003). The granitic magma may result from partial melting of meta-sedimentary middle-crust at about 750°C due to dehydration (Harris & Massey, 1994). The crystallisation temperatures for the EIA granitoids calculated in the present study by using the zircon and apatite saturation methods are 728°C–848°C for the granodiorites, 797°C–880°C for the microgranites and 704°C–809°C for the leucogranites. Magmatic to sub-solidus temperatures calculated by Toksoy-Köksal (2016) (granodiorite: 615–783°C, microgranite: 464–565°C, leucogranite: 456–482°C), on the other hand, infer late stage recrystallisation during slow cooling. Emplacement depths of the granitoids are between 6 and 16 km for the granodiorites, and ≥ 10 km depths for the microgranites and the leucogranites (e.g. Toksoy-Köksal, 2016).

As a result, this study reveals that the EIA granitoids were generated in a collisional to post-collisional setting with a pronounced crustal signature. These granitoids are suggested to be formed from partial melting of crustal dominated sources triggered by crustal thickening during the closure of the İzmir-Ankara-Erzincan branch of the Neotethyan Ocean by obduction of ophiolitic units on to the passive edge of the Tauride-Anatolide Platform.

8. Conclusions

The EIA granitoids, namely granodiorite, microgranite and leucogranite, show distinct field, petrographical, whole-rock element and isotopic geochemical characteristics. The main magmatic phase in the area is respresented by the granodiorites, which exhibit a mainly I-type character, with essential hornblende, biotite and plagioclase contents, and abundant mafic microgranular enclaves. The microgranites and the leucogranites, on the other hand, are S-type two-mica granitoids. The geochemical data collectively show that these three granitoid types are non-cogenetic.

Whole-rock geochemistry, including Sr-Nd isotope data, reveals that the S-type microgranites with high $^{87}Sr/^{86}Sr$ and low εNd have a crustal source with an insignificant mantle input, while the S-type leucogranites display higher mantle input than the microgranites. The I-type granodiorite, on the other hand, has higher $^{87}Sr/^{86}Sr$ and lower εNd with respect to typical I-type granitoids, thus indicating higher crustal contribution in its petrogenesis.

Mean LA-ICP-MS zircon $^{206}Pb/^{238}U$ ages for the Ekecikdağ granitoids are reported as 80 to 85 Ma. Moreover, LA-ICP-MS Lu-Hf isotope data obtained from the rims and younger zones of the zircons from the Ekecikdağ granitoids reveal their crustal nature (i.e. $\varepsilon Hf_{(t)}$: −1.3 ± 0.5 to −8.8 ± 0.5).

The zircon and apatite saturation methods give the crystallisation temperatures for the EIA granitoids as 728°C–848°C for the granodiorites, 797°C–880°C for the microgranites and 704°C–809°C for the leucogranites.

As a result, it is suggested that the EIA granitoids were formed by partial melting of a crustal dominated igneous source. However, all the granitoids have a mantle input, which is the highest in granodiorites and the lowest in the microgranites. Understanding of the nature and evolution of the collisional granitoids in Central Anatolia is important not only to establish its contribution to the geodynamic evolution of Central Anatolia and surrounding Alpine area, but also to understand the systematics of collisional magmatic systems.

Acknowledgments

I wish to thank the Scientific and Technical Research Council of Turkey (TUBITAK; project code 106Y066) for supporting the whole rock geochemical and LA-ICP-MS U-Pb analyses. I am indebted to Radiogenic Isotope Laboratory of Middle East Technical University Central Laboratory for Sr-Nd isotope analyses, Geological Survey of Denmark and Greenland (GEUS) for zircon U-Pb analyses, Johann Wolfgang Goethe Universität, Institut für Geowissenschaften for zircon Lu-Hf isotope analyses and GFZ-Potsdam for accessing to SEM and CL imaging and EPMA analyses. I would like to thank Semih Gürsu, Serhat Köksal, Andreas Möller, Dirk Frei, Axel Gerdes and M. Cemal Göncüoğlu for their contributions in the analyses and discussion of data. I am thankful to two anonymous reviewers who made valuable comments and help to improve the manuscript.

Disclosure statement

No potential conflict of interest was reported by the author.

Funding

This work was supported by the Scientific and Technical Research Council of Turkey [106Y066].

ORCID

Fatma Toksoy-Köksal http://orcid.org/0000-0003-3187-4838

References

Akıman, O., Erler, A., Göncüoğlu, M. C., Güleç, N., Geven, A., Türeli, T. K., & Kadıoğlu, Y. K. (1993). Geochemical characteristics of granitoids along the western margin of the Central Anatolian Crystalline Complex and their tectonic implications. *Geological Journal*, *28*, 371–382.

Amelin, Y., Lee, D.-C., Halliday, A. N., & Pidgeon, R. T. (1999). Nature of the Earth's earliest crust from hafnium isotopes in single detrital zircons. *Nature*, *399*, 252–255.

Anderson, D. L. (2007). The eclogite engine: Chemical geodynamics as a Galileo thermometer. In G. R. Foulger & D. M. Jurdy (Eds.), *Plates, plumes and planetary processes* (pp. 430). Boulder, Colorado: Geological Society of America Special Paper. doi:10.1130/2007.2430(03)

Batchelor, R. A., & Bowden, P. (1985). Petrogenetic interpretation of granitoid rock series using multcationic parameters. *Chemical Geology*, *48*, 43–55.

Boztuğ, D. (1998). Post-collisional central Anatolian alkaline plutonism, Turkey. *Turkish Journal of Earth Sciences*, *7*, 145–165.

Boztuğ, D. (2000). S-I-A-type intrusive associations: Geodynamic of significance of synchronism between metamorphism and magmatism in central Anatolia, Turkey. In E. Bozkurt, J. A. Winchester, & J. D. A. Piper (Eds.), *Tectonics and magmatism in Turkey and the surrounding area* (Vol. 173, pp. 441–458). London, UK: Geological Society of London Special Publication.

Boztuğ, D., & Arehart, G. B. (2007). Oxygen and sulfur isotope geochemistry revealing a significant crustal signature in the genesis of the post-collisional granitoids in central Anatolia, Turkey. *Journal of Asian Earth Sciences*, *30*, 403–416.

Boztuğ, D., Arehart, G. B., Platevoet, B., Harlavan, Y., & Bonin, B. (2007c). High-K, calc-alkaline I-type granitoids from the composite Yozgat batholith generated in a post-collisional setting following continent-oceanic island arc collision in central Anatolia, Turkey. *Mineral and Petrology*, *91*, 191–223.

Boztuğ, D., Harlavan, Y., Arehart, G. B., Satır, M., & Avcı, N. (2007b). K–Ar age, whole-rock and isotope geochemistry of A-type granitoids in the Divrigi-Sivas region, eastern-central Anatolia, Turkey. *Lithos*, *97*, 193–218.

Boztuğ, D., Jonckheere, R. C., Heizler, M., Ratschbacher, L., Harlavan, Y., & Tichomirova, M. (2009). Timing of post-obduction granitoids from intrusion through cooling to exhumation in central Anatolia, Turkey. *Tectonophysics*, *473*, 223–233.

Boztuğ, D., Temiz, H., Jonckheere, R., & Ratschbacher, L. (2008). Punctuated exhumation and foreland basin formation and infilling in (circum)–Central Anatolia (Turkey) associated with the Neo-Tethyan closure. *Turkish Journal of Erath Sciences*, *17*, 673–684.

Boztuğ, D., Tichomirowa, M., & Bombach, K. (2007a). ^{207}Pb–^{206}Pb single-zircon evaporation ages of some granitoid rocks reveal continent-oceanic island arc collision during the Cretaceous geodynamic evolution of the central Anatolian crust, Turkey. *Journal of Asian Earth Sciences*, *31*, 71–86.

Chappell, B. W., & White, A. J. R. (1974). Two contrasting granite types. *Pacific Geology*, *8*, 173–174.

Chappell, B. W., White, A. J. R., & Wyborne, D. (1987). The importance of residual source material (restite) in granite petrogenesis. *Journal of Petrology*, *28*, 1111–1138.

Chauvel, C., Lewin, E., Carpentier, M., Arndt, N. T., & Marini, J. C. (2008). Role of recycled basalt and sediment in generating the Hf-Nd mantle array. *Nature Geoscience*, *1*, 64–67.

Chen, W., Xu, Z., Chen, M., & Yu, Y. (2016). Multiple sources for the origin of the early Cretaceous Xinxian granitic batholith and its tectonic implications for the western Dabie orogeny, eastern China. *Mineralogy and Petrology*, *110*, 29–41.

De La Roche, H., Leterrier, J., Grandclaude, P., & Marchal, M. (1980). A classification of volcanic and plutonic rocks using R1R2-diagram and major-element analyses - Its relationships with current nomenclature. *Chemical Geology*, *29*, 183–210.

Delibaş, O., Genç, Y., & De Campos, C. P. (2011). Magma mixing and unmixing related mineralization in the Karacaali magmatic complex, Central Anatolia, Turkey. In A. N. Sial, J. S. Bettencourt & C. P. De Campos (Eds.), *Granite-Related Ore Deposits* (Vol. 350, pp. 149–173). London, UK: Geological Society of London Special Publications.

Deniz, K., & Kadıoğlu, Y. K. (2016). Assimilation and fractional crystallization of foid-bearing alkaline rocks: Buzlukdağ intrusives, Central Anatolia, Turkey. *Turkish Journal of Earth Sciences*, *25*, 341–366.

Düzgören-Aydın, N. S., Malpas, J., Göncüoğlu, M. C., & Erler, A. (2001). A review of the nature of magmatism in central Anatolia during the mesozoic post-collisional period. *International Geological Review*, *43*, 695–710.

Erler, A., Akıman, O., Unan, C., Dalkılıç, B., Geven, A., & Önen, P. (1991). The petrology and geochemisty of the Kırşehir massif magmatic rocks in Kaman (Kırşehir) and Yozgat regions. *Doga-Türk Yerbilimleri Dergisi*, *15*, 76–100.

Erler, A., & Göncüoğlu, M. C. (1996). Geologic and tectonic setting of the Yozgat Batholith, northern Central Anatolian Crystalline Complex, Turkey. *International Geological Review*, *38*, 714–726.

Floyd, A. F., Göncüoğlu, M. C., Winchester, J. A., & Yalınız, M. K. (2000). Geochemical character and tectonic environment of neotetyan ophiolitic fragments and metabasites in the Central Anatolian Crystalline Complex, Turkey. *Geological Society,London, Special Publications*, *173*, 183–202.

Göncüoğlu, M. C., Erler, A., Toprak, V., Olgun, E., Yaliniz, K., Kuşçu, I., … Dirik, K. (1993). *Geology of the central part of the Central Anatolian Massif: Part III, geological evolution of the tertiary basin of the Central Kızılırmak* (Report No: 3313). Ankara, Turkey: Turkish Petroleum Company.

Göncüoğlu, M. C., Erler, A., Toprak, V., Yaliniz, K., Olgun, E., & Rojay, B. (1992). *Geology of the western part of the Central Anatolian Massif: Part II, Central Part* (Report No: 3155). Ankara, Turkey: Turkish Petroleum Company.

Göncüoğlu, M. C., Köksal, S., & Floyd, P. A. (1997a). Post-collisional A-type magmatism in the Central Anatolian Crystalline Complex: Petrology of the İdiş Dağı Intrusives (Avanos Turkey). *Turkish Journal of Earth Sciences*, *6*(2), 65–76.

Göncüoğlu, M. C., Kozlu, H., & Dirik, K. (1997b). Pre-Alpine and Alpine terranes in Turkey: Explanatory notes to the terrane map of Turkey. *Ann. Geol. Pays Helleniques*, *37*, 515–536.

Göncüoğlu, M. C., Toprak, G. M. V., Kuşçu, I., Erler, A., & Olgun, E. (1991). *Geology of the western part of the Central Anatolian Massif: Part I, Southern Part* (Report No: 2909). Ankara, Turkey: Turkish Petroleum Company.

Göncüoğlu, M. C., & Türeli, T. K. (1994). Alpine collisional-type granitoids from Western Central Anatolian Crystalline Complex, Turkey. *Journal of Kocaeli University, Earth Science Section*, *1*, 39–46.

Görür, N., Oktay, F. Y., Seymen, İ., & Şengör, A. M. C. (1984). Paleotectonic evolution of Tuzgölü basin complex, Central Turkey. In J. E. Dixon & A. H. F. Robertson (Eds.), *The geological evolution of the Eastern Mediterranean* (Vol. 17, pp. 81–96). Geological Society of London: Special Publications.

Gray, C. M. (1984). An isotopic mixing model for the origin of granitic rocks in southeastern Australia. *Earth and Planetary Science Letters*, *70*, 47–60.

Güleç, N., & Kadıoğlu, Y. K. (1998). Relative involvement of mantle and crustal components in the Ağaçören granitoid (central Anatolia – Turkey): Estimates from trace element and Sr-isotope data. *Chemie der Erde*, *58*, 23–37.

Gürsu, S., Möller, A., Göncüoğlu, M. C., Köksal, S., Demircan, H., Köksal, F. T., … Sunal, G. (2015). Neoproterozoic continental arc volcanism at the northern edge oft he Arabian Plate, SE Turkey. *Precambrian Research*, *258*, 208–233.

Harris, N., & Massey, J. (1994). Decompression and anatexis of the Himalayan metapelites. *Tectonics*, *13*, 1537–1546.

Harrison, T. M., & Watson, E. B. (1984). The behaviour of apatite during crustal anatexis: Equilibrium and kinetic considerations. *Geochimica et cosmochimica acta*, *48*, 1467–1477.

Hauri, E. H., Wagner, T. P., & Grove, T. L. (1994). Experimental and natural partitioning of Th, U, Pb and other trace elements between garnet, clinopyroxene and basaltic melts. *Chemical Geology*, *117*, 149–166.

Hinsbergen, V. D. J. J., Maffione, M., Plunder, A., Kaymakcı, N., Ganerød, M., Hendriks, B. W. H., … Vissers, R. L. M. (2016). Tectonic evolution and paleogeography of the Kırşehir Block and the Central Anatolian Ophiolites, Turkey. *Tectonics*, *35*, 983–1014.

Hofmann, A. W. (1997). Mantle geochemistry: The message from oceanic volcanism. *Nature*, *385*, 219–229.

Hofmann, A. W. (2003). Sampling mantle heterogeneity through oceanic basalts: Isotopes and trace elements. In R. W. Carlson (Ed.), *The mantle and core, col 2, treatise on geochemistry* (pp. 61-101). Amsterdam: Elsevier.

Hofmann, A. W., & Jochum, K. P. (1996). Source characteristics derived from very incompatible trace elements in Mauna Loa and Mauna Kea basalts, Hawaii scientific drilling project. *Journal of Geophysical Research*, *101*(B5), 11831–11839.

Hughes, C. J. (1973). Spilites, keratophyres and igneous spectrum. *Geological Magazine*, *109*(6), 513–527.

İlbeyli, N. (2005). Mineralogical–Geochemical constraints on intrusives in central Anatolia, Turkey: Tectono-magmatic evolution and characteristics of mantle source. *Geological Magazine*, *142*, 187–207.

İlbeyli, N., Pearce, J. A., Thirlwall, M. F., & Mitchell, J. G. (2004). Petrogenesis of collision-related plutonics in central Anatolia, Turkey. *Lithos*, *72*, 163–182.

Kadıoğlu, Y. K., Ateş, A., & Güleç, N. (1998). Structural interpretation of gabbroic rocks in Ağaçören Granitoid, Central Turkey: Field observations and aeromagnetic data. *Geological Magazine*, *135*(02), 245–254.

Kadıoğlu, Y. K., Dilek, Y., & Foland, K. A. (2006). Slab break-off and syncollisional origin of the Late Cretaceous magmatism in the Central Anatolian Crystalline Complex, Turkey. In Y. Dilek & S. Pavlides (Eds.), *Postcollisional tectonics and magmatism in the Mediterranean region and Asia* (Vol. 409, pp. 381–415). Geological Society of America Special Paper, US.

Kadıoğlu, Y. K., Dilek, Y., Güleç, N., & Foland, K. A. (2003). Tectonomagmatic evolution of bimodal plutons in the Central Anatolian Crystalline Complex, Turkey. *Journal of Geology*, *111*, 671–690.

Keay, S., Collins, W. J., & Mcculloch, M. T. (1997). A three component Sr-Nd mixing model for granitoid genesis, Lachlan Fold Belt, Eastern Australia. *Geology*, *25*, 307–310.

Kemp, A. I. S., Hawkesworth, C. J., Foster, G. L., Paterson, B. A., Woodhead, J. D., Hergt, J. M., … Whitehouse, M. J. (2007). Magmatic and crustal differentiation history of granitic rocks from Hf-O isotopes in zircon. *Science*, *315*, 980–983.

Koçak, K., Isık, F., Arslan, M., & Zedef, V. (2005). Petrological and source region characteristics of ophiolitic hornblende gabbros from the Aksaray and Kayseri regions, central Anatolian crystalline complex, Turkey. *Journal of Asian Earth Sciences*, *25*(6), 883–891.

Köksal, S., & Göncüoğlu, M. C. (2008). Sr and Nd isotopic characteristics of some S-, I- and A-type granitoids from Central Anatolia. *Turkish Journal of Earth Sciences*, *17*, 111–127.

Köksal, S., Göncüoğlu, M. C., & Floyd, P. A. (2001). Extrusive members of postcollisional A-type magmatism in central Anatolia: Karahidir volcanics, Idisdagi-Avanos area, Turkey. *International Geology Review*, *43*, 683–694.

Köksal, S., Möller, A., Göncüoğlu, M., . C., Frei, D., & Gerdes, A. (2012). Crustal homogenization revealed by U-Pb zircon ages and Hf isotope evidence from the Late Cretaceous granitoids of the Agaçören intrusive suite (Central Anatolia/Turkey). *Contributions to Mineralogy and Petrology*, *163*, 725–743.

Köksal, S., Romer, R. L., Göncüoğlu, M. C., & Toksoy-Köksal, F. (2004). Timing of post-collisional H-type to A-type granitic magmatism: U–Pb titanite ages from Alpine central Anatolian Granitoids (Turkey). *International Journal of Earth Sciences*, *93*, 974–989.

Köksal, S., Toksoy-Köksal, F., & Göncüoğlu, M. (2017). Petrogenesis and geodynamics of plagiogranites from Central Turkey (Ekecikdağ/Aksaray): New geochemical and isotopic data for generation in an arc basin system within the northern branch of Neotethys. *International Journal of Earth Sciences*, *106*, 1181–1203.

Köksal, S., Toksoy-Köksal, F., Göncüoğlu, M. C., Möller, A., Gerdes, A., & Frei, D. (2013). Crustal source of the Late Cretaceous Satansarı monzonite (Central Anatolia/Turkey) and its significance for the Alpine geodynamic evolution. *Journal of Geodynamics*, *65*, 82–93.

Lefebvre, C., Barnhoorn, A., van Hinsbergen, D. J. J., Kaymakci, N., & Vissers, R. L. M. (2011). Late Cretaceous extensional denudation along a marble detachment fault zone in the Kırşehir massif near Kaman, Central Turkey. *Journal of Structural Geology*, *33*, 1220–1236.

Lefebvre, C., Peters, K., Wehrens, P., Brouwer, F. M., & van Roermund, H. L. M. (2015). Thermal and extensional exhumation history of a high-temperature crystalline complex (Hırkadağ Massif, Central Anatolia). *Lithos*, *238*, 156–173.

Maas, R., Kamenetsky, V., Nicholls, I. A., & Steele, D. (2001). The petrogenesis of mafic S-type magmas: Quenched melt inclusions in phenocrysts of a Silurian dacite (Lachlan Fold Belt). In B. W. Chappell & P. D. Fleming (Eds.), *S-type granites and related rocks* (Vol. 02, pp. 77–78). Australia: Australian Geological Survey Organisation Record

Maniar, P. D., & Piccoli, P. M. (1989). Tectonic discrimination of granitoids. *Geological Society of America Bulletin*, *101*, 635–643.

Okay, A. I., Satır, M., Maluski, H., Siyako, M., Monié, P., Metzger, R., & Akyüz, S. (1996). Paleo-and Neo-Tethyan events in northwestern Turkey: Geologic and geochronologic constraints. In A. Yin & T. M. Harrison (Eds.), *The tectonic evolution of Asia* (pp. 420–441). Cambridge, U.K.: Cambridge Univ. Press.

Otlu, N., & Boztuğ, D. (1998). The coexistence of the silica oversaturated (Alkos) and undersaturated (Alkus) rocks in the kortundag and baranadag plutons from The Central Anatolian alkaline plutonism, E Kaman/Nw Kirsehir, Turkey. *Turkish Journal of Earth Sciences*, *7*, 241–257.

Özgül, N. (1976). Some geological aspects of the taurides orogenic belt. *Bulletin of the Geological Society of Turkey*, *19*, 65–78. in Turkish with English abstract.

Pearce, J. A., Harris, N. B. W., & Tindle, A. G. W. (1984). Trace element discrimination diagrams for the tectonic interpretation of granitic rocks. *Journal of Petrology*, *25*, 956–983.

Petermann, M., Hirschmann, M. M., Hametner, K., Gunther, D., & Schmidt, M. W. (2003). Experimental determination of trace element partitioning between garnet and silica-rich liquid during anhydrous partial melting of MORB-like eclogite. *Geochemistry, Geophysics, Geosystems*, *5*. doi:10.1029/2003gc000638

Reichardt, H., & Weinberg, R. F. (2012). The dike swarm of the Karakoram shear zone, Ladakh, NW India: Linking granite source to batholith. *Geological Society of America Bulletin*, *124*, 89–103.

Richardson, S. H., Erlank, A. J., Duncan, A. R., & Reid, D. L. (1982). Correlated Nd, Sr and Pb isotope variation in Walvis Ridge basalts and implications for the evolution of their mantle source. *Earth and Planetary Science Letters*, *59*, 327–342.

Şengör, A. M., & Yılmaz, Y. (1981). Tethyan evolution of Turkey: A plate tectonic approach. *Tectonophysics*, *75*, 181–241.

Spitz, G., & Darling, R. (1978). Major and minor element lithogeochemical anomalies surrounding the Louvem copper deposit, Val d'Or, Quebec. *Canadian Journal of Earth Sciences*, *15*, 1161–1169.

Sun, S. S., & Mcdonough, W. F. (1989). Chemical and isotopic systematics of ocean basalts: Implication for mantle composition and processes. In A. D. Saunders & M. J. Norry (Eds.), *Magmatism in ocean basins* (Vol. 42, pp. 313–345). London, UK: Geological Society of London Special Publication.

Tatar, S., & Boztuğ, D. (1998). Fractional crystallization and magma mingling/mixing processes in the monzonitic association in the SW part of the composite Yozgat batholith (Şefaatli-Yerköy, SW Yozgat). *Turkish Journal of Earth Sciences*, *7*, 215–230.

Thiéblemont, D., & Cabanis, B. (1990). Utilisation d'un diagramme (Rb/100)—Tb—Ta pour la discrimination geochimique et l'etude petrogenetique des roches magmatiques acides. *Bulletin De La Societé Géologique De France (8)*, *VI*(1), 23–35.

Tiepolo, M., & Tribuzio, R. (2008). Petrology and U-Pb zircon geochronology of amphibole-rich cumulates with sanukitic affinity from Husky Ridge (northern Victoria Land, Antarctica); insights into the role of amphibole in the petrogenesis of subduction-related magmas. *Journal of Petrology*, *49*, 937–970.

Toksoy-Köksal, F. (2016). Petrology of the Ekecikdağ Igneous Association (Central Anatolia): Mineral chemistry perspective. *Yerbilimleri*, *37*(2), 139–178. in Turkish with English abstract.

Toksoy-Köksal, F., Göncüoğlu, M. C., & Yalınız, M. K. (2001). Petrology of the Kurancali phlogopite metagabbro: An island arc-type ophiolitic sliver in the Central Anatolian Crystalline Complex. *International Geology Review*, *43*, 624–639.

Toksoy-Köksal, F., Oberhaensli, R., & Göncüoğlu, M. C. (2009). Hydrous aluminosilicate metasomatism in an intra-oceanic subduction zone: Implications from the Kurancali (Turkey) ultramafic-mafic cumulates within the Alpine Neotethys Ocean. *Mineralogy and Petrology*, *95*, 273–290.

Türeli, T. K. (1991). Geology, petrography and geochemistry of Ekecikdağ plutonic rocks (Aksaray Region Central Anatolia) (Ph.D. Thesis). Middle East Technical University, Dept. of Geological Engineering. p. 194. (unpublished).

Türeli, T. K., Göncüoğlu, M. C., & Akıman, O. (1993). Ekecikdağ Granitoyidinin Petrolojisi ve Kökeni (Orta Anadolu Kristalen Kütlesi Batısı). *Bulletin of the Mineral Research and Exploration*, *115*, 15–28.

Villaseca, C., Downes, H., Pin, C., & Barbero, L. (1999). Nature and composition of the lower continental crust in Central Spain and the granulite–granite linkage: Inferences from granulitic xenoliths. *Journal of Petrology*, *40*(10), 1465–1496.

Watson, E. B., & Harrison, T. M. (1983). Zircon saturation revisited: Temperature and composition effects in a variety of crustal magma types. *Earth and Planetary Science Letters*, *64*, 295–304.

Whitney, D. L., & Hamilton, M. A. (2004). Timing of high grade metamorphism in central Turkey and the assembly of Anatolia. *Journal of the Geological Society London*, *161*, 823–828.

Whitney, D. L., Teyssier, C., Dilek, Y., & Fayon, A. K. (2001). Metamorphism of the Central Anatolian Crystalline Complex, Turkey: Influence of orogen-normal collision vswrench-dominated tectonics on P-T-t paths. *Journal of Metamorphic Geology*, *19*, 411–432.

Whitney, D. L., Teyssier, C., Fayon, A. K., Hamilton, M. A., & Heizler, M. (2003). Tectonic controls on metamorphism, patial melting, and intrusion; timing and duration of regional metamorphism and magmatism in the Niğde Masif, Turkey. *Tectonophysics*, *376*, 37–60.

Winchester, J. A., & Floyd, P. A. (1977). Geochemical discrimination of different magma series and their differentiation product using immobile elements. *Chemical Geology*, *20*, 325–343.

Workman, R. K., & Hart, S. R. (2005). Major and trace element composition of the depleted MORB mantle (DMM). *Earth and Planetary Science Letters*, *231*, 53–72.

Workman, R. K., Hart, S. R., Jackson, M., Regelous, M., Farley, K. A., Blusztajn, J., … Staudigel, H. (2004). Recycled metasomatized lithosphere as the origin of the Enriched Mantle II (EM2) end-member: Evidence from the Samoan Volcanic Chain. *Geochemistry, Geophysics, Geosystems*, *5*, Q04008.

Yalınız, M. K., Aydın, N. S., Göncüoğlu, M. C., & Parlak, O. (1999). Terlemez quartz monzonite of Central Anatolia (Aksaray-Sarıkaraman): Age, petrogenesis and geotectonic implications for ophiolite emplacement. *Geological Journal*, *34*, 233–242.

Yalınız, M. K., Göncüoğlu, M. C., & Özkan-Altıner, S. (2000). Formation and emplacement ages of the SSZ-type Neotethyan ophiolites in Central Anatolia, Turkey: Paleotectonic implications. *Geological Journal*, *35*, 53–68.

Yılmaz, S., & Boztuğ, D. (1998). Petrogenesis of the Çiçekdağ Igneous Complex, north of Kırşehir, Central Anatolia, Turkey. *Turkish Journal of Earth Sciences*, *7*, 185–199.

Zindler, A., & Hart, S. R. (1986). Chemical geodynamics. *Annual Review of Earth and Planetary Sciences*, *14*, 493–571.